

Improved Manufacturing Methods of Bovine Femur Samples for Ultrasonic
Testing and Assessment of Materials Through Contact Angle Measurement

A Senior Project

presented to

the Faculty of the Biomedical Engineering Department
California Polytechnic State University, San Luis Obispo

In Partial Fulfillment

of the Requirements for the Degree

Bachelor of Science in Biomedical Engineering

by

Kevin Mathew Lopez Galang

September, 2011

Abstract

At California Polytechnic State University of San Luis Obispo (Cal Poly), the Biomedical Engineering department (BMED) requires its students to take the course listed as “BMED 420: Principles of Biomaterial Designs.” BMED 420 has a required laboratory section every week throughout the duration of the course that is meant to be a supplemental tool for learning. During the lab sections, students perform experiments and exercises that are currently being implemented in the industry. Despite accuracy of the methods and experiments relative to their use in the industry, there is always room for improvement. The objective of this project will illustrate my procedural approach to the improvement of Lab F— Ultrasonic Biomaterial Analysis and the expansion of Lab B— Contact Angle measurement. More specifically, I will provide a step by step account of the creation of new bovine femur bone samples and test their efficacy using the same ultrasonic testing methods the students are familiar with. I will also go through the analysis of existing and new materials for the Contact Angle Measurement methods to verify their use in the expansion of Lab B— Contact Angle Measurement.

1. Introduction

Biomaterials may be defined as artificial or natural materials that can mimic, store, come into contact with or are integrated with living biological cells or fluid (Menzies et. al., "The Impact of Contact Angle on the Biocompatibility of Biomaterials."). A few examples of biomaterials or devices with biomaterials are: Titanium hip joint prosthetics, tissue engineered skin grafts, tissue engineered heart-valves, contact lenses, artificial hearts, breast implants, silicone rubber finger joints, and ceramic dental implants.

At Cal Poly, the class BMED 420, is listed as the "Principles of Biomaterial Design" with a course description as follows: "Fundamentals of materials science as applied to bioengineering design. Natural and synthetic polymeric materials. Materials characterization and design. Wound repair, blood clotting, foreign body response, transplantation biology, biocompatibility of materials, tissue engineering. Artificial organs and medical devices. Government regulations." The breakdown of the class is 3 hours of lecture with 1 hour of lab per week for the duration of the quarter. In lecture at the beginning of every class, Dr. Kristen Cardinal presents the class with learning objectives, or LO's. These LO's serve as the main message that Dr. Cardinal is trying to teach during each lecture. Although all the LO's are important, there are few of them which I found to be the most useful and that served as my inspiration for this project: Describe different types of biomaterials and explain how the field of biomaterials is evolving, Provide specific examples of how metals and ceramics are currently being used and improved for use as biomaterials, Discuss specific examples of polymers used for drug delivery and tissue engineering applications, Summarize ISO 10993 evaluation techniques for determining local and systemic responses at acute and chronic time point, List and justify design considerations for a given application, Provide at least two examples of surface modification approaches currently being used in industry, Clearly state the goals of biomaterial evaluation and outline the progression of testing methods, State the role of the FDA with regard to medical device regulation and summarize the type of data that the FDA typically reviews based on device classification (BMED 420 - Lecture and Lab - Winter 2011.).

Another way students gain knowledge about biomaterials in the BMED 420 course is through the 1 hour of lab they complete per week. Each week, students are split up into their lab groups and perform experiments and participate in activities that supplement the material being taught in lecture. There are 7 laboratories that the students complete throughout the quarter. Each lab, with a brief description, is listed below

Lab A – Tensile Testing familiarizes students with tensile testing its ability to obtain important material properties, like elastic modulus.

Lab B – Contact angle allows students to perform contact angle measurements with various liquids on different polymeric materials to obtain the critical surface energies of the tested materials.

Lab C – Bone Crushing has students placing chicken bone under a flexural test to observe the strength and stiffness of natural bone.

Lab D – Material Selection familiarizes students with a materials database known as CES; with this program, students learn about the importance of optimizing material selection for a given application.

Lab E – Histology Lab is an introduction to decellularized cells and is hands on walkthrough of the process of histology; students are responsible for their own sectioning and staining of their histology slides.

Lab F – Ultrasonic Biomaterial Analysis involves the ultrasonic analysis of bovine femur to calculate the elastic modulus of bone.

Lab G – Bioquant Lab introduces students to an automated method of histological analysis of equine cortical bone; students determine the porosity and volume fraction of osteons (BMED 420 - Lecture and Lab - Winter 2011.)

Despite the multitude of knowledge that students gain from executing the existing laboratory exercise each week, there are a number of labs that can be improved. Specifically, Lab B – Contact Angle Lab, and Lab F – Ultrasonic Biomaterial Analysis are two labs that contain room for improvement. The Contact Angle Lab enhancement lies in the materials being tested. As of now, students are limited to only performing contact angle measurements with four solutions on two materials. Since the purpose Contact Angle Lab is to analyze the surface energy of the material, I decided to test 3 new materials that can be added to the lab. The major setbacks of the Ultrasonic Biomaterial Analysis are the bone samples used for testing. The bones samples are not ideal for perform ultrasound test, their angles and contours skew the data of the ultrasound test. This project will include the testing and analysis of 3 new materials to be added to Lab B, and the step-by-step account of creating new bone samples and the ultrasound testing used to validate the use of the new samples.

2. Ultrasound

2.1 INTRODUCTION

The purpose of this lab is to compute the elastic modulus of bovine femur using ultrasonic analysis and to determine if there is any variance in the elastic modulus between the medial, lateral, cranial and caudal parts of the bone. (BMED 420 - Lecture and Lab - Winter 2011.)¹ Ultrasonic Testing is currently used to test for mechanical properties of bone and metals, because of its non-invasive and non-destructive testing nature. Ultrasound testing has been used as an advancement in the diagnosis of osteoporosis, a bone disease that plagues more than 20 million people in America (Muller et. al. "Nonlinear Ultrasound Can Detect Accumulated Damage in Human Bone.").

The Panametrics NDT ultrasound machine utilizes the send/receive configuration, which allows the detection of material properties The sender generates sound energy and propagates the sound wave through the material where the opposite wall of the material reflects the wave back to the transducer. Equation 1 shows the relationship between the distance the wave has to travel, the time of travel, and the velocity of the wave; where v is the wave velocity, d is the distance the wave travels, and t is length of time the wave has travelled. The factor of two takes into account for the wave traveling twice the distance due to reflection (*NDT Resource Center*. NDT).

$$v = 2 \frac{d}{t}$$

Equation 1 –Velocity of the ultrasound wave

The current problem with the ultrasound lab is the geometry of the bone samples. The current bone samples are not cubic in any way; they have slightly rounded edges and non-parallel faces. (Figure 1a) The erratic and non-cubic shape of the old bones reflects the sound waves in all different directions. Ergo, the data obtained from using the equation will be inaccurate. Because the waves are not bouncing straight back to the transducer the non-flat surface increases travel time of the sound wave and skews the ultrasonic readings, and the velocity within the material will appear to be slower than it should. The ideal shape of the new bones would be cubes or rectangular prisms. The flat and parallel surfaces would produce the most accurate ultrasound results because the sound wave will reflect normal to the surface of contact. With the direct return of the sound wave, the computed velocity will be most accurate. The Panametrics NDT Ultrasound machine uses a send/receive configuration; therefore, when the bone samples are more cubic is when the ultrasonic testing will produce the most accurate data. (Figure 1b) Grimal

et. al. obtained plate-like bone samples for ultrasonic testing of human femur bone samples to obtain the mechanical properties of the bone. The rectangular prismatic shapes of the plates supports the importance of the flat cubic geometry of the bone samples for ultrasonic testing. (Figure 2)(Grimal et. al., "Assessment of Cortical Bone Elasticity and Strength: Mechanical Testing and Ultrasound Provide Complementary Data.")

The main objective of this section is to provide a step-by-step look at the process of machining new bone samples and testing the effectiveness of the bone samples, via ultrasound testing, as new additions to the Ultrasonic Biomaterial Analysis lab.

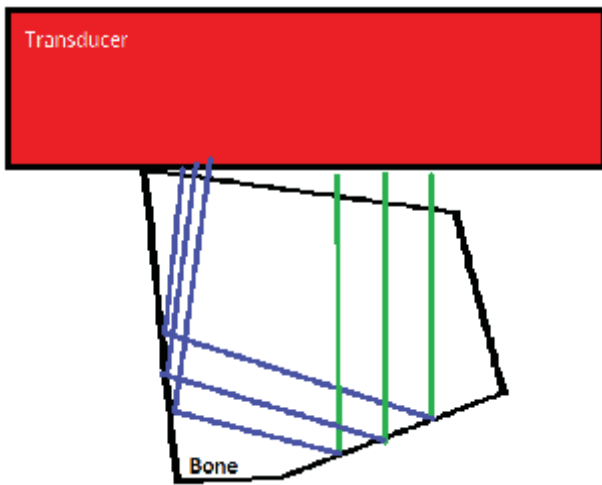


Figure 1a –Drawing of the behavior of wave propagation within the old bone samples. The transducer sends a sound wave through the bone and the wave reflects off of the opposite end of the bone. The wave reflects normal to surface it comes in contact with. If the reflecting surface is not flat, then the wave travels through the bone sample longer, and skews the results. The green lines are the sending signal and the blue lines are the receiving lines.

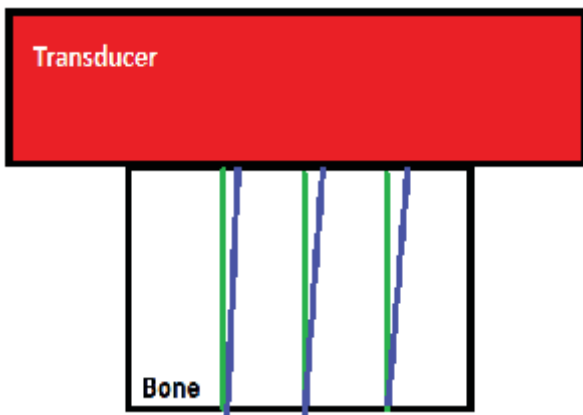


Figure 1b –Drawing of the behavior of wave propagation within the new bones. Because the new bones are flat, the ultrasound waves will reflect normal to the bones surface and will return directly back to the transducer. The prompt and direct return of the sound wave will produce the best results for ultrasonic testing. The blue lines are angled to illustrate the return of the sound wave to the transducer

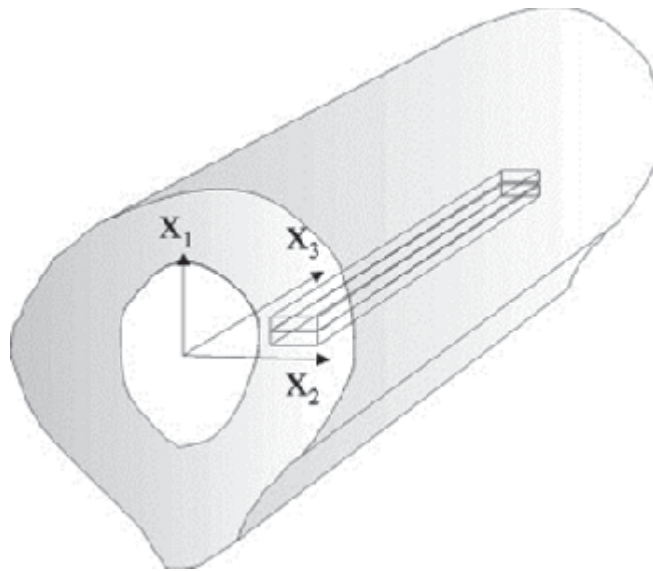


Figure 2 – Grimal et. al. obtain plate-like bone samples for their ultrasonic testing to obtain the best results. The rectangular prismatic shape ensures that the shape of the samples do not interfere with the travel time or pathway of the sound waves.

2.2 MATERIALS AND METHODS

The main materials used in the new method of creating bone sample were a vertical bandsaw and a belt sander. The acquisition and the manufacturing of the bovine femur samples will be described below.

The materials used for the ultrasound testing were the 12 new bone samples, micro-calipers for dimensional measurements, a graduated cylinder to measure the displacement of the bone samples, mineral oil to prep the samples for the ultrasound tests, bone holding apparatus to hold the bones in place during the ultrasound testing, and lastly the Panametrics NDT ultrasound testing machine to perform the ultrasound tests.

A. Creating New Bone Samples

The bone samples being used for ultrasonic testing were cut down from a whole bovine femur. To obtain the bovine femur, call the local butcher shop or the meat department of a local grocery shop; I called the meat department at Spencer's grocery store and they provided me with both a whole cow femur and tibia. (Figure 3)



Figure 3— Whole bovine tibia (top bone) and femur (bottom bone). These bones are easily attainable through the local grocer or butcher shop

Before any cutting could occur, I scraped off the excess meat, fat, and various tissues left on the femur was scraped off using a razor blade and a small paring knife— I only scraped off the tissue from the diaphysis because the two epiphysis ends were going to be cut off. After I cleaned the diaphysis, I labeled the femur's Anterior, Posterior, Medial, and Lateral faces with a pencil or sharpie; I used anatomical images as a reference for the correct direction. (Figure 4a & Figure 4b). Next I used the vertical band saw to cut both epiphyses ends off and leaving only the diaphysis section and its labeled faces. (Figures 5a-5c)

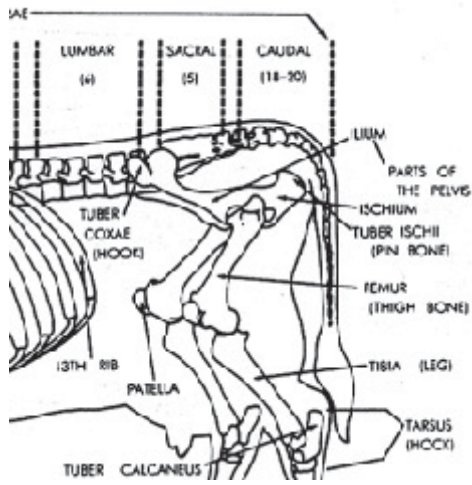


Figure 4a— Anatomical chart of a bovine skeleton. The chart is used as a reference for the correct labeling of the whole bovine femur

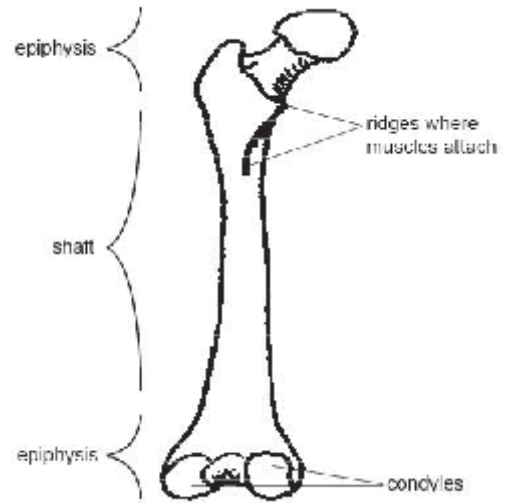


Figure 4b— Anatomical picture of a bovine femur. The image is used as a reference for the correct labeling of the whole bovine femur



Figure 5a—Labeling of the lateral face of the bovine femur after all the excess tissue and meat has been scraped off, and the two epiphyses ends have been cut off.



Figure 5b—Distal end of the diaphysis after the distal and proximal epiphyses were cut with a vertical band.



Figure 5c— Proximal end of the diaphysis after the distal and proximal epiphyses were cut with a vertical band.

At this point, the diaphysis is treated as a cylinder, and the next objective is to turn the cylinder into a rectangular prism. In order to transform the round cylindrical edges into flat rectangular prismatic edges is by flattening them; this was done with a belt sander. The sanding was performed on all four sides and I immediately relabeled the sides so that I could maintain the correct anatomical direction. (Figures 6a-6d)



Figure 6a—Posterior face of diaphysis after it has been flattened down with a belt sander



Figure 6b—Anterior face of diaphysis after it has been flattened down with a belt sander



Figure 6c—Medial face of diaphysis after it has been flattened down with a belt sander



Figure 6d—Lateral face of diaphysis after it has been flattened down with a belt sander

Since I was trying to create cubic samples out of each direction of the diaphysis, I felt that it would be easier to create cubes out of the diaphysis if each I worked with each side separately. Thus I used the band saw to cut the flattened diaphysis into four separate sections. (Figures 7a-7b)



Figure 7a—The diaphysis from the Proximal-Distal view. The outline below the “M” is the medial face of the diaphysis before it is separated from the rest of the diaphysis with a vertical band.



Figure 7b—The diaphysis from the Proximal-Distal view The Medial section has been cut off from the remaining diaphysis with the vertical band

With each of the newly cut sections, I determined where the bone was the thickest and outlined the section with a pencil. Then cut the trim the edges of the sections to obtain a more rectangular prismatic shape. (Figures 8a-8b) I sanded the inner surface of the bone as well to eliminate the rough and unsmooth texture of bone (Figure 9a); the results were that both the inner and outer surface are relatively parallel to each other. (Figure 9b).



Figure 8a—The thickest portion of the Medial section. The excess bone was removed via vertical band saw. The edges of the section were flattened and squared off with the vertical belt sander



Figure 8b—The thickest portion of the Anterior section. The excess bone was removed via vertical band saw and the edges of the section were flattened and squared off with the vertical belt sander



Figure 9a—The underside or inner portion of the Medial section. The rough remaining bone of the inner surface of all the sections was flattened and smoothed out with a vertical belt sander

Figure 8b—The underside or inner portion of the Medial section. The

and smoothed out with a vertical belt sander

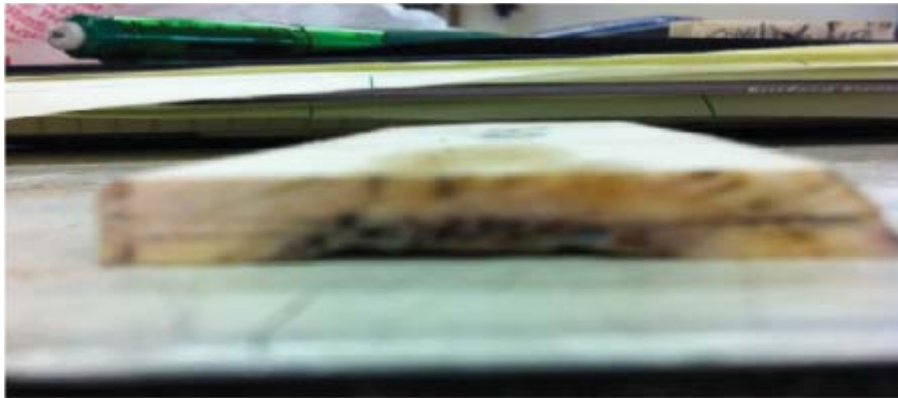


Figure 9b—The Medial section laying flat against a table top after the edges and both inner and outer surfaces have been flattened with a belt sander.

Once the rectangular prismatic or cubic geometry of the cut was reached, I outlined four smaller sections. It was critical to label the remaining bone sections with the appropriate X, Y, or Z axis labels; the anterior-posterior direction is the X-axis, the medial-lateral direction is the Y-axis, and the proximal-distal direction is the Z-axis. (Figures 10a-10c)



Figure 10a – The remaining anterior section in its rectangular prismatic form. The outline on the bone surface is for the machining of four smaller bone samples. The X surface is labeled to ensure that the directional orientation of the bone samples is not lost



Figure 10b – The remaining anterior section in its rectangular prismatic form. The Z surface is labeled to ensure that the directional orientation of the bone samples is not lost



Figure 10c – The remaining anterior section in its rectangular prismatic form. The Z surface is labeled to ensure that the directional orientation of the bone samples is not lost

Finally, I cut along the outlines of the of the larger bone sections to obtain the new cubic bone samples or rectangular prismatic bone samples. Some larger sections were able to only produce three cubic or rectangular prismatic samples, and if some of the larger sections produced four samples, the best three were selected. (Figure 11)



Figure 11 – The newly cut bone samples that will undergo ultrasonic testing according to the “Lab F- Ultrasonic Biomaterial Analysis” protocol. All the new samples are either cubes or rectangular prisms.

B. Measuring Bone Parameters

First I measured the x, y, and z thickness for each sample in each of the four sample categories (Medial, Caudal, Cranial, and Lateral) with micrometer calipers. (Figure 12) Secondly, treating the bone samples as cubes or rectangular prisms, I calculated the volume of each sample with the following equations l^3 or $l \times w \times h$, respectively. Next I measured the displacement of each sample with graduated cylinder by observing the difference of the waterline before and after the bone sample is dropped in. (Table I) I measured the mass of each bone sample with the micro balance (Figure 13); the volume and mass will be used to calculate the density of each bone sample. (Table II)



Figure 12— The microcalipers are they measure the new bone samples to the nearest hundredth millimeter



Figure 13 – The microbalance used to measure the mass of the bone samples to the nearest ten thousandth gram

Table I— The measured dimensions in the X, Y, and Z directions for all the bone samples. The volume was calculated with the measured dimensions. The displacement was measured with a graduated cylinder.

	X	Y	Z	Volume (cm ³)	Displacement (ml)
Medial					
1	6.38	8.9	14.53	0.825042	0.7
2	6.52	7.12	15.6	0.724189	0.5
3	6.5	7.66	15.42	0.767762	0.5
Lateral					
1	9.96	9.2	11.82	1.08309	1.0
2	9.79	9.2	11.04	0.994351	1.0
3	9.59	9.42	10.14	0.916025	1.0
Anterior					
1	6.64	8.66	13.22	0.760182	0.5
2	6.1	13	10.06	0.797758	0.5
3	6.66	8.6	13.02	0.745734	0.5
Posterior					
1	6.9	12.52	10.4	0.898435	1.0
2	7	12.56	11.5	1.01108	1.0
3	6.92	12.56	12.28	1.067319	1.0

Table II— The measured mass of the bone samples in grams and then converted to kilograms. The density was calculated with the calculated volume from Table I. The density is then converted to kg/m³ in order to maintain the correct units with future calculations

	Mass (g)	Mass (kg)	Density (g/cm ³)	Density (kg/m ³)
Anterior				
1	1.3287	0.001329	1.610463	1610.463
2	1.5675	0.001568	1.899902	2164.489
3	1.4804	0.00148	1.794332	1928.202
Posterior				
1	1.7811	0.001781	2.158798	1644.461
2	1.984	0.001984	2.404725	1995.272
3	2.1123	0.002112	2.560232	2305.941
Lateral				
1	1.9908	0.001991	2.412967	2618.847
2	1.8707	0.001871	2.267398	2344.947
3	1.6898	0.00169	2.048137	2265.957
Medial				
1	1.6861	0.001686	2.043652	1876.707
2	1.5658	0.001566	1.897842	1548.641
3	1.5259	0.001526	1.849481	1429.657

C. Ultrasound Testing

To start the ultrasound testing, I placed the bone samples in the bone holding apparatus; tightening the threaded screws so that the bone sample is held firmly on both sides. (Figure 14) While the bone is firmly secured in the bone holding apparatus, I used a cotton swab to place a generous amount of mineral oil on the surface of the bone sample that is up for ultrasound testing. Once Panametrics NDT ultrasound machine is set up and calibrated—as stated in the “Lab F - Ultrasound”, I placed the transducer directly on top of the surface of the bone sample that is oriented vertically and pushed down firmly with the transducer. I made sure there is nothing below the bone sample that comes in contact with the surface directly beneath the bone. (Figure 15) I made sure that the “echo-echo” is set to one peak. For best results, I either adjusted the gain or the range, or added more mineral oil. When the Panametrics NDT screen shows two green peaks, I adjusted “Gate 1” so that the solid red gate is centered and measures the width of the top of the second peak; the first peak created will be from the natural noise that comes from the transducer. (Figure 16) Then I pressed the “2nd Function” key, and then the velocity key; from here a window will pop up asking for the thickness of the bone sample. I entered the thickness that corresponds with the direction being subjected to the ultrasound test; for example, if the transducer is placed on the surface labeled “X,” then enter the thickness of the bone in the X-direction. The velocity of the ultrasound wave will then appear in the upper left corner of the data on the Panametrics NDT screen. (Table III) Because there were three ultrasonic tests taken per direction per sample, I calculated the average velocity in each direction per sample for the computation of the stiffness coefficients of each bone sample. With the equation $C_{ii} = \rho(V_{ii})^2$, I used the calculated ultrasound average velocities and the calculated density to compute the stiffness coefficient for that particular direction of the bone sample. I used the data from Table IV to perform the one-way ANOVA testing in minitab.

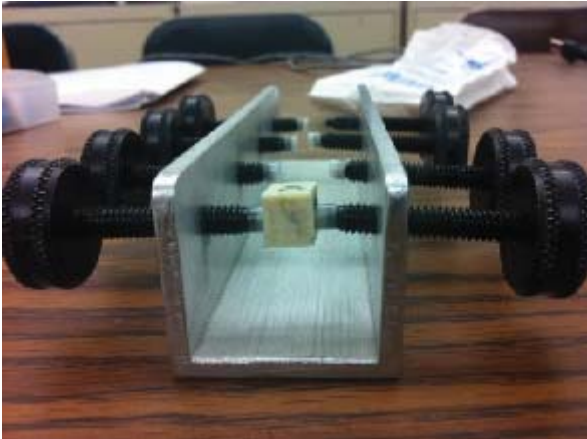


Figure 14— The old bone holding apparatus being used to hold one of the new bone samples for ultrasonic testing.

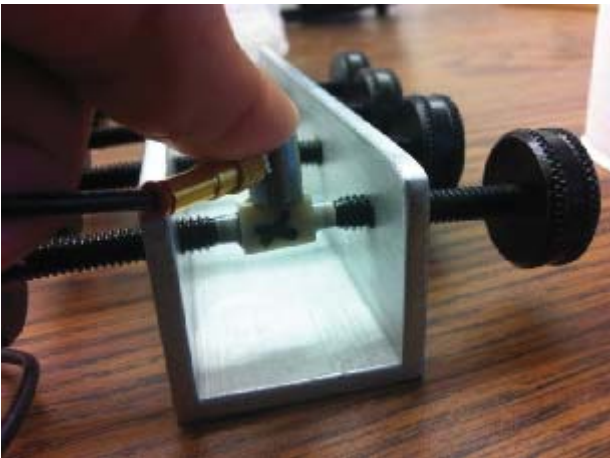


Figure 14— The Panametrics NDT Ultrasound Machine transducer is placed firmly on the top surface of the bone. Because the plastic caps on the threaded screws of the apparatus are flat, they are able to firmly apply pressure on the newly flattened and parallel edges of the bone samples; this sufficient side wall pressure counter acts the downward force being applied to the bones during ultrasonic testing. Make sure that there is nothing that comes in contact with the underside of the bone samples for the most accurate results



Figure 15— The screen of the Panametrics NDT Ultrasound machine as it subjects a bone sample to ultrasonic testing. The peak on the left is noise from the transducer as it sends the signal through the bone. The second peak is the result of the sound waves coming back to the transducer. The red bar is “gate 1,” this gate will be used to measure the width of the top of the second peak.

Table III— The Measured ultrasonic velocities for the bone samples. Threeultrasound tests were taken in each direction for all samples. X1, Y1, and Z1 correspond to the first ultrasonic tests while X2, Y2, and Z2 correspond to the second, and X3, Y3, and Z3 correspond to the third tests

	X1	Y1	Z1	X2	Y2	Z2	X3	Y3	Z3
Lateral									
1	2155	2866	3344	2832	2914	3363	2964	2769	3368
2	2766	2733	3363	2799	2744	3505	2793	2750	3503
3	2833	2736	3599	2899	2738	3612	2902	2756	3589
Medial									
1	2235	4169	3956	2239	4159	3970	2244	4188	3970
2	2675	3292	3949	2629	3196	3864	2626	3200	3864
3	2714	3567	3896	2642	3447	3759	3864	2634	3443
Anterior									
1	2909	3187	4180	2707	3204	4170	2699	3201	4170
2	2915	3095	3789	2943	3285	3866	2922	3283	3934
3	2905	3203	3973	2688	3203	3991	2641	3165	3991
Posterior									
1	2866	3317	3772	2914	3321	3654	2890	3321	3775
2	2789	3221	3755	2750	3299	3677	2740	3294	3683
3	2708	3152	3660	2714	3259	3799	2698	3259	3799

2.3 RESULTS

The mean velocities of the ultrasound testing ranged from 2239.333-3073.333 m/s in the X direction, 2743.333-4172 m/s in the Y direction, and 3358.333-4173.333 m/s in the Z direction. (Table IV) $C_{1,1}$, which corresponds to the stiffness coefficient of the Medial-1 sample in the X-direction, uses the average velocity in the X direction of the Medial-1 sample. The average velocities in each direction for each sample were used to compute the stiffness coefficients in the X, Y, and Z directions for all twelve bone samples for increased accuracy. The range of stiffness coefficients in the X direction is 9.41096285-18.76865798 GPa, the range in the Y direction is 14.78645-32.66519 GPa, and the range in the Z direction is 27.38915-32.47343 GPa. (Table V)

Table IV – Calculated average velocities from Table III in the X, Y, and Z directions for all bone

Average	X	Y	Z
Lateral			
1	2650.333	2849.667	3358.333
2	2786	2742.333	3457
3	2878	2743.333	3600
Medial			
1	2239.333	4172	3965.333
2	2643.333	3229.333	3892.333
3	3073.333	3216	3699.333
Anterior			
1	2771.667	3197.333	4173.333
2	2926.667	3221	3863
3	2744.667	3190.333	3985
Posterior			
1	2890	3319.667	3733.667
2	2759.667	3271.333	3705
3	2706.667	3223.333	3752.667

Table V – Calculated stiffness coefficients in the X, Y, and Z directions, their calculated averages , and their standard deviations

	X	Y	Z
Lateral			
1	18.39548332	21.26661	29.53642
2	18.20099802	17.63492	28.0241
3	18.76865798	17.05331	29.3668
Average	18.45504644	18.65162	28.97577
Stdev	0.288479258	2.283249	0.828522
Medial			
1	9.41096285	32.66519	29.5091
2	10.820682	16.15015	23.46231
3	13.50365411	14.78645	19.56496
Average	11.24509965	21.2006	24.17879
Stdev	2.079093116	9.952013	5.010639
Anterior			
1	12.37179266	16.46366	28.04896
2	18.53966507	22.45623	32.30017
3	14.52552347	19.62568	30.62028
Average	15.1456604	19.51519	30.32314
Stdev	3.130349803	2.99781	2.141124
Posterior			
1	13.73470535	18.12227	22.92423
2	15.19551176	21.35264	27.38915
3	16.89342403	23.95844	32.47343
Average	15.27454705	21.14445	27.5956
Stdev	1.580841821	2.92365	4.777945

ANOVA TESTING

I performed the “One-Way ANOVA” test in Minitab just as it was stated in the protocol. The “Factor” column, which contains the treatment values is the left column, while the “Response” is the right column. Table VI is an example of the “One-Way ANOVA” test for the $C_{1,1}$ values. Below, are the outputs for the “One-Way ANOVA” tests for $C_{1,1}$, $C_{2,2}$, and $C_{3,3}$. The ultimate objective of the ANOVA testing was to test the variance of the mechanical properties within the anterior, posterior, medial, and lateral sections of the bone. Table VII is a summary table of the results of the ANOVA testing results.

Table VI – Minitab set for the “One-Way Anova” testing for $C_{1,1}$. The left column is the “treatment” while the right column is the “response”

C1-T	C2
L1	18.3955
L1	18.201
L1	18.7687
L2	9.411
L2	10.8207
L2	13.5037
L3	12.3718
L3	18.5397
L3	14.5255
L4	13.7347
L4	15.1955
L4	16.8934

Table VII— The statistically determined “P-values” for the $C_{1,1}$, $C_{2,2}$, and $C_{3,3}$ one-way ANOVA tests performed in minitab

	P-Value
$C_{1,1}$	0.017
$C_{2,2}$	0.923
$C_{3,3}$	0.271

As the ANOVA test results show— please refer to Appendix A for the raw ANOVA test produced by Minitab, for the $C_{1,1}$ the test yielded a p-value of 0.017, which shows that the X direction stiffness coefficients are significantly different for each section of the bovine femur. For the Y direction, the ANOVA yielded a p-value of 0.923, which shows that the y-direction stiffness coefficients are not significantly different for each section of the bovine femur. The Z direction ANOVA test yielded a p-value of 0.271, which shows that the z-direction stiffness coefficients are not significantly different for each section of the bovine femur. (Table VIII)

2.4 DISCUSSION

The use of ultrasound for bone analysis allows for a detailed look into the mechanical properties of the bone without compromising the quality of the bone samples. It is completely non-invasive and non-destructive with respect to the bone, although destructive methods were used to create the bone samples. Furthermore, the bone specimen needed for ultrasonic analysis can vary in size and shape as long as the samples retain relatively cuboidal or rectangular prismatic geometry. The low restriction of sample parameters allows for the easy creation of new bone samples. Finally, with ultrasonic analysis it is possible to obtain measurements of multiple anisotropic properties from one sample.

The main objective of this portion of my senior project was to produce new bone samples for the Ultrasound Lab, which is part of the BMED 420 curriculum. The improvement of the newly created bones lies in their geometry. The new bone samples are all either rectangular prisms or cuboidal, and having parallel sides leads to more accurate readings from the ultrasound tests because of the “send-receive” behavior of the transducer. Another benefit to the newly created bones is the number of samples available. By increasing the number of samples, there can be more tests that can be performed on the bones and more data can be collected. Secondly, with twelve samples, there are backups in case one of the samples gets lost or begins to wear away.

To validate the effectiveness of these newly created bones, the Ultrasound Lab was to be performed on the new bone samples. Lasaygues et. al. also performed an ultrasound test on bovine femur and obtained the following ranges for their bovine femur stiffness coefficients : 14-21 GPa in the radial, or X and Y, direction, and 20-25 GPa in the longitudinal or Z direction. The new bone samples created in this project fell in the range of 11.25-21.14 GPa in the X and Y direction and 24.18-30.32 GPa in the Z direction. Lasaygues et. al. tested their bovine bone samples with a more complex ultrasound test, which might explain the differences in data. A second reason for the difference in data can be attributed to the samples; Lasaygues et. al. performed their ultrasound tests while the bone still retained its wet properties, but in my case I was unaware that the bones needed to be frozen between testing or manufacturing. This caused the bones to dry out and exhibit its dry properties (Lasaygues et. al. “Ultrasonic Characterization of Orthotropic Elastic Bovine Bones”).

After the ultrasound testing of the bones, there was a distinguishable (and expected) material property that was discovered, bone is anisotropic. Anisotropy is when a material’s properties are directionally dependent; the mechanical properties measured along the x axis will differ than those measured along the y and z axes. The range of the stiffness coefficient further supports the rationale that bone is anisotropic. One reason why this may occur is because bone is subjected to a greater force in the z-direction for longer durations of time. The body thus adapts to the z-direction force by making bone stronger in the z-direction by remodeling itself to add more dense layers. Another reason for the directional dependency of bone is the numerous layers that comprise bone. The individual layers each contribute their own material property. Also, each layer is placed in different locations and at different thicknesses within the bone. Despite being the non-homogeneity of bone, there was only a slight difference in the velocities of the x-direction and y-direction. Adding to the benefit of ultrasound, the use of low frequency allowed for a longer wavelength, which gave the ability to penetrate all the way through the layers of the bone providing for a comprehensive analysis.

Although this portion of my senior project was to improve on this lab, there were some problems, and there still exists limitations. The most difficult obstacle to overcome was shaping the bones. The goal of the new bone samples was to create 12 1cm^3 pieces. Unfortunately, I was not able to create perfect 1cm cubes, and this occurred for two main reasons. First, the belt sander and vertical band saw became less precise as the piece got smaller and the smaller pieces made it exceedingly difficult to shape. Secondly, as the machining progressed, it became more of a priority to obtain the rectangular geometry as opposed to the exact 1cm cubes. The bones inner and outer surfaces have extreme contours and rough texture that needed to be sanded down, but trying to create flat surfaces on both the inside and outside of the femur greatly diminished the thickness in some sections of the bone.

A secondary improvement for the ultrasound lab was to create a new bone holding apparatus for the lab. The original bone holding apparatus as shown in Figure 13 only applies pressure to the sides of the bone sample, thus it is only effective if the sample exhibits rectangular prism or cuboidal shape. The idea behind my new design

involved increasing the adjustability of the holding apparatus by adding adjustable shelves and new bottom supports. As it turns out however, because the new bone samples are relatively cubic, the original bone holding apparatus holds up quite nicely. Although I did not fully create a new bone holding apparatus, I believe it is important to document my progress as it might prove itself useful in the future. Figures 16 – 20 show a couple of new designs that I and BMED Technician David Laiho came up with. Figure 16 involved one moving adjustable side grip with the wall of the channel on the opposite side acting as the second side grip, and the two bottom vertical supports would counteract the downward force applied during the ultrasound test. Figure 17 consisted of two adjustable side grips with two and two horizontal bottom supports. Figure 18 involves one adjustable side grip with the opposite facing wall acting as the second side grip and two cylindrical bottom supports. Figure 19 was the final design, and going to be manufactured until I discovered that the current bone samples worked well with the original bone holding apparatus. Figure 19 involves a toggle clamp, with an adjustable end piece, acting as the main side grip while the opposite wall would act as the second side grip. The red “L” in Figure 19 represents an L-bracket that would act as a shelf that would combat the downward force exerted on the sample. The increased adjustability lies in the movable head piece of the toggle clamp, and in the addition of the shelf; the shelf would counter act the downward force of the student while not interfering with the ultrasound test thus allowing for non- cubic bone samples.

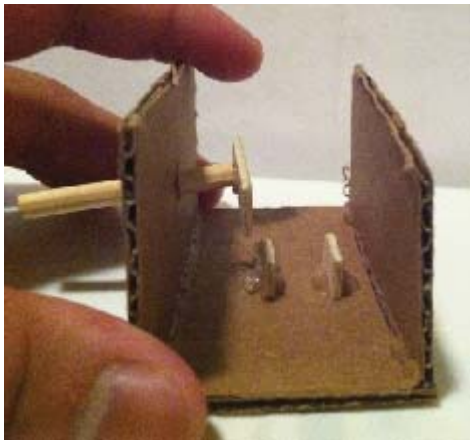


Figure 16 – Cardboard design 1 for the new bone holding apparatus. The bone sample would be gripped from the side while it's supported from the bottom during the ultrasound tests.

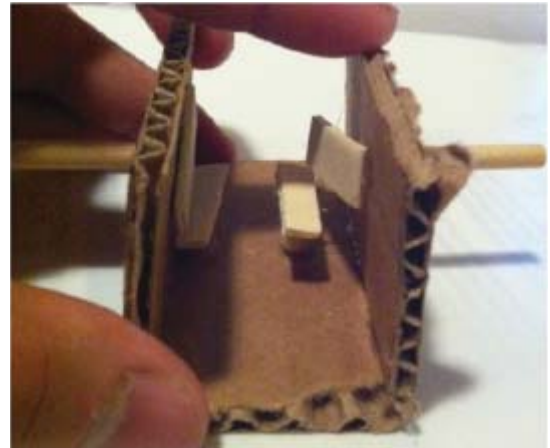


Figure 17 – Cardboard design 2 for the new bone holding apparatus. The bone sample would be gripped from the side while it's supported from the bottom during the ultrasound tests.

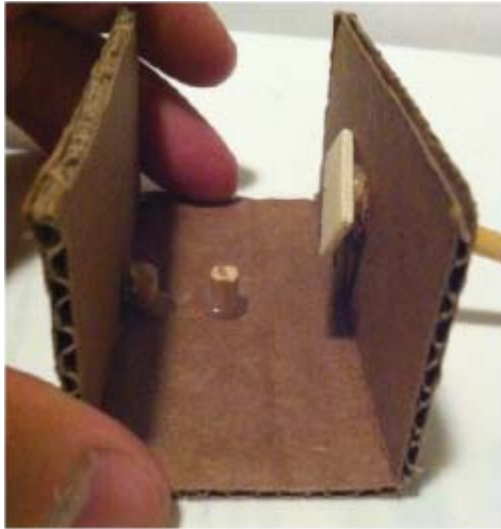


Figure 18– Cardboard design 3 for the new bone holding apparatus. The bone sample would be gripped from the side while it's supported from the bottom during the ultrasound tests.

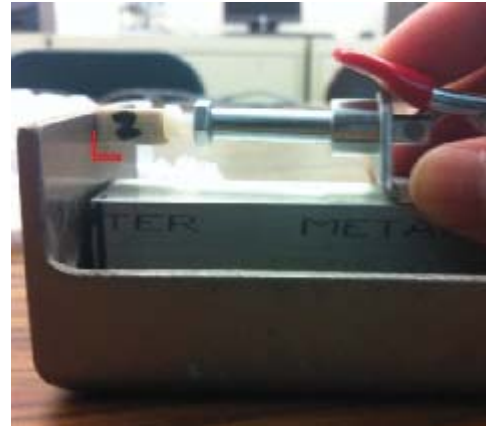


Figure 19 – The final design of the new bone holding apparatus. The toggle clamp and the side wall will act as the side grips, while the L-shaped shelf (the “Red L” in the picture) will support the bone sample from the bottom

In conclusion, I was able to obtain newly better shaped bone samples that proved to be efficient with the original bone holding apparatus. The new bone samples were also tested using the ultrasound machine and produced a tremendous amount of applicable data. Although the bones are not ideal in their geometry, they will prove themselves to be a rather large improvement upon the ultrasound lab.

3. Contact Angle

3.1 INTRODUCTION

The purpose of this lab is to measure various contact angles of a selection of liquids on polymeric materials in order to the critical surface energy using a Zisman plot. Another goal of this lab is to help students understand how critical surface energies differ among biomaterials and the reason for these differences (BMED 420 - Lecture and Lab - Winter 2011). Contact angle is defined the angle between a liquid-vapor interface and the solid surface tangent to the interface (Deganello et. al. "Numerical simulation of dynamic contact angle using a force based formulation."). The foundation of the theory behind the contact angle is Young's Contact equation— Equation 2 below, where θ_E is the unique, equilibrium contact angle, σ_{LV} is the liquid–vapour interfacial tension, σ_{SV} the solid–vapour interfacial tension, and σ_{SL} the solid–liquid interfacial tension (Beatty and Smity, “Fractional wettability and contact angle dynamics in burned water repellent soils.”).

$$\sigma_{LV} \cos(\theta_E) = \sigma_{SV} - \sigma_{SL}$$

Equation 2 – Young's Contact Angle

Equation 2 is what makes contact angle measurements possible. The contact angle measurements that will be taken will allow for the analysis of the surface energy of the solid material. Hydrophobic materials have a contact angle greater than 90° , poor wettability and low solid surface free energy; hydrophilic materials have a contact angle less than 90° , high wettability, and high solid surface free energy (Lyndon and Jones, “The Impact of Contact Angle on the Biocompatibility of Biomaterials.”). (Figure 20-21)

Revamping the Contact Angle lab mainly involves a wider selection of materials that can be tested using the contact angle measurements. The goal of this section is to explore the contact angle measurements of three new materials: Glass, Titanium, and Nylon. The analysis of the results will be used to justify if any of the three new materials are eligible for use in the Contact Angle lab.

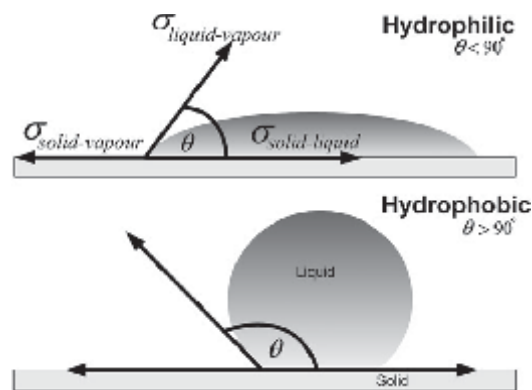


Figure 20—Examples of contact angles. Hydrophilic angles are less than 90° while hydrophobic angles are greater than 90°

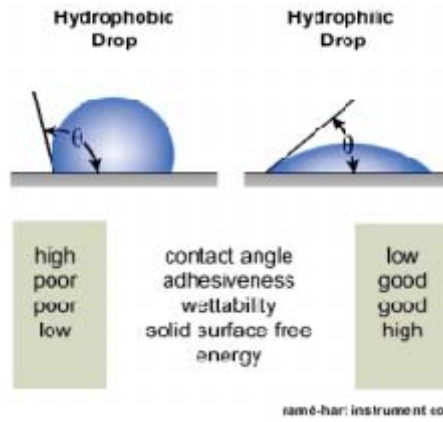


Figure 21— Comparison table of the different properties of hydrophobic and hydrophilic materials

3.2 MATERIALS AND METHODS

The solutions used for the contact angle measurements were Methyl Salicate, Diethylene Glycol, DI Water, and 70% Ethanol. The liquid surface energy of 70% Ethanol had to be calculated using the for the “rule of mixtures” where V_{f1} is the volume fraction of the liquid and γ_1 is the surface energy of the liquids.^[3] All other liquid surface energies were given. The new materials up for testing were Glass (glass slides), Titanium, and Nylon (fabric). The contact angle measurements were taken with the VCA Optima machine and software. (Equation 3)

$$\gamma_{mixture} = V_{f1}\gamma_1 + (100-V_{f1})\gamma_2$$

Equation 3— The equation used to determine the surface energy of 70% Ethanol

A. Contact Angle measurements

I first set up the contact angle testing area by turning on all VCA optima machines, computers and starting up the VCA optima software. Second, with each sample, I wiped the testing surface clean with a paper towel, I made sure to wear latex gloves when I handled the samples because the oil from skin would contaminate the samples. Third, I placed the sample on the adjustable platform of the VCA optima machine. With the VCA optima program open, I adjusted the platform so that the surface of the sample and the needle are visible in the program window. Next I clicked the droplet button and made sure that the droplet was set at .75microlitres. As the droplet formed on the needle, I SLOWLY raised the surface of the sample so that the droplet touched and adhered to the sample’s surface, then I lowered the sample. I waited approximately 3 seconds then took a snapshot of the liquid-solid interface with the snapshot function. Next I calculated the contact angle of the droplet either through the auto-calculate function of the program or manually by placing the L(left) icon at the left of the edge of the droplet, then working clockwise, placing the T(top) icon at the top of the droplet, then finally placing the R(right) icon at the right edge of the droplet. If the angle appeared to be small, I used the low angle function if the angle of the droplet.(Figure 22a-Figure22h) For better data, I recorded the contact angle of three droplets for each solution for each material and calculated the average contact angles for both the left and right directions for each solution and material. (Table IX-XI)



Figure 22b—The contact angle measurement of DI Water on the surface of the Titanium sample. The left and right contact angles are measured with the VCA Optima program. The left and right angles were both 97.20°

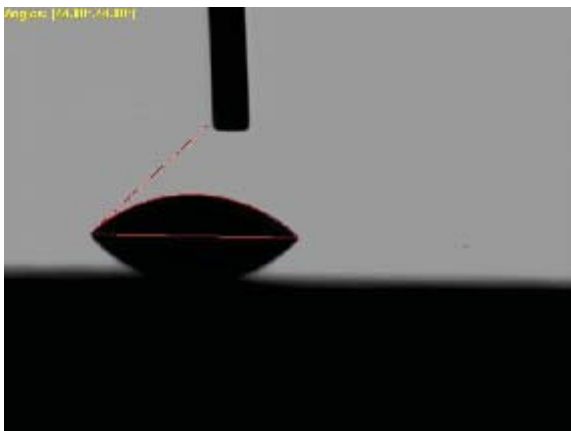


Figure 22a—The contact angle measurement of 70% Ethanol on the surface of the titanium sample. The left and right contact angles are measured with the VCA Optima program. The left and right angles were both 40.0°

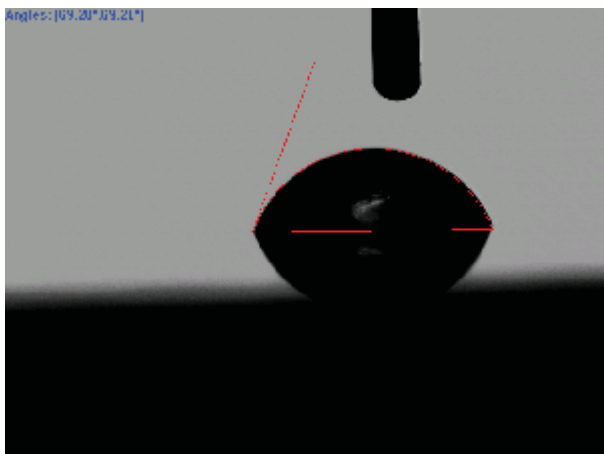


Figure 22c—The contact angle measurement of Diethylene Glycol on the surface of the Titanium sample. The left and right contact angles are measured with the VCA Optima program. The left and right angles were both 69.2°

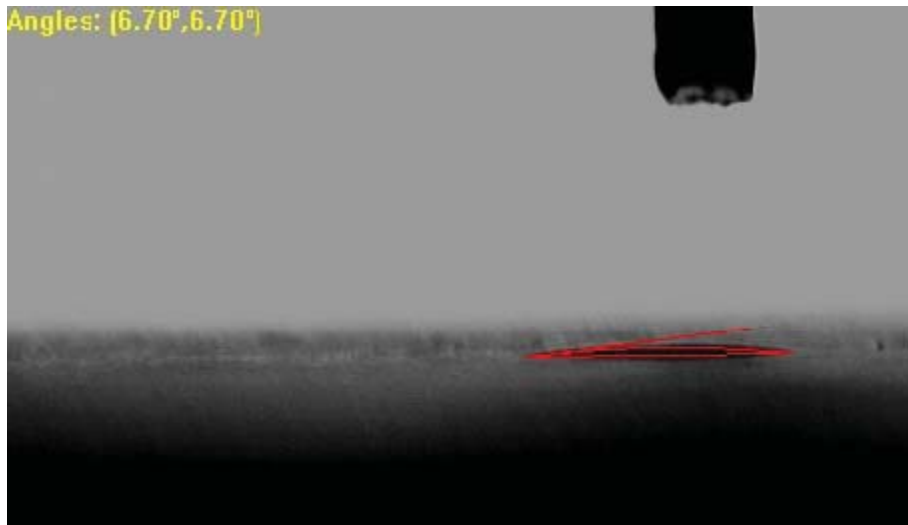


Figure 22c—The contact angle measurement of Methyl Salicate on the surface of the Titanium sample. The left and right contact angles are measured with the VCA Optima program. The left and right angles were both 6.70° . The droplet size was adjusted to be $1.5\mu\text{L}$ because at $.75\mu\text{L}$, the droplet would almost immediately evaporate

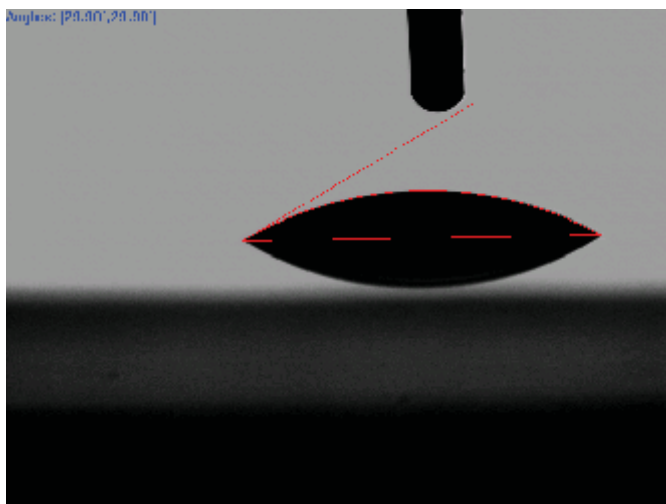


Figure 22d—The contact angle measurement of Diethylene Glycol on the surface of the Glass sample. The left and right contact angles are measured with the VCA Optima program. The left and right angles were both 29.90° .

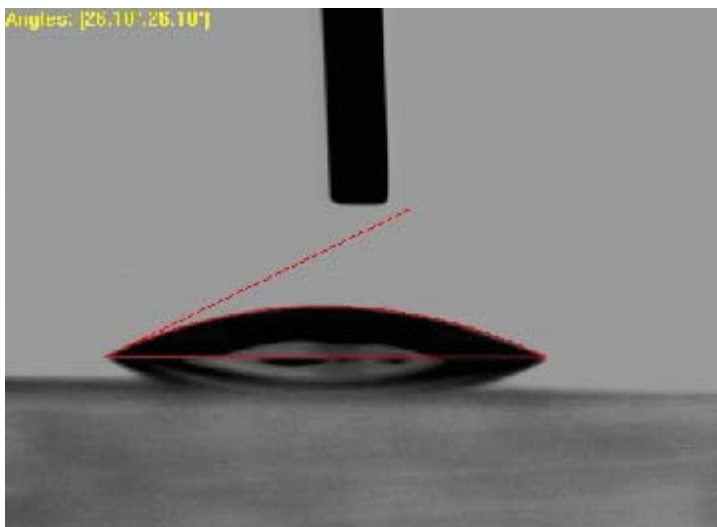


Figure 22e—The contact angle measurement of 70% Ethanol on the surface of the Glass sample. The left and right contact angles are measured with the VCA Optima program. The left and right angles were both 26.10° .

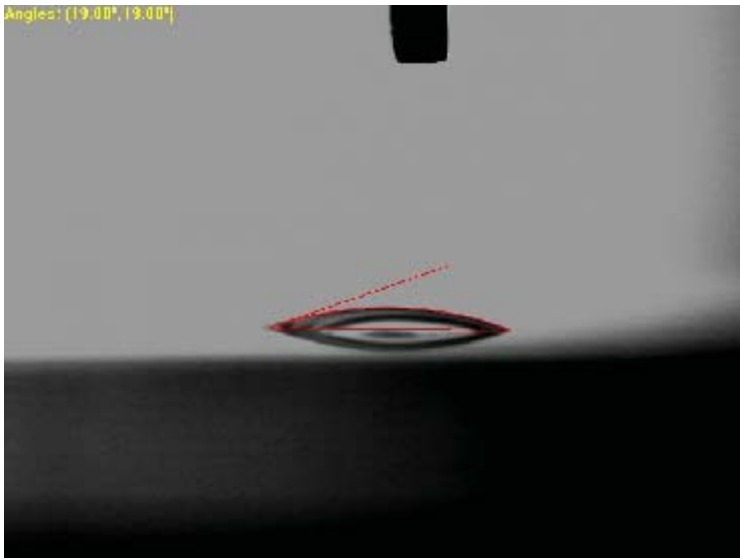


Figure 22f—The contact angle measurement of Methyl Salicate on the surface of the Glass sample. The left and right contact angles are measured with the VCA Optima program. The left and right angles were both 19.00°

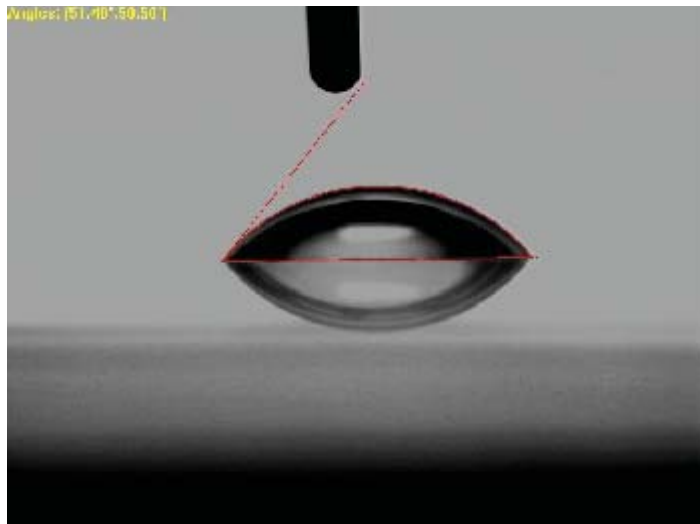


Figure 22g—The contact angle measurement of DI Water on the surface of the Glass sample. The left and right contact angles are measured with the VCA Optima program. The left and right angles were 51.40° and 50.50° .

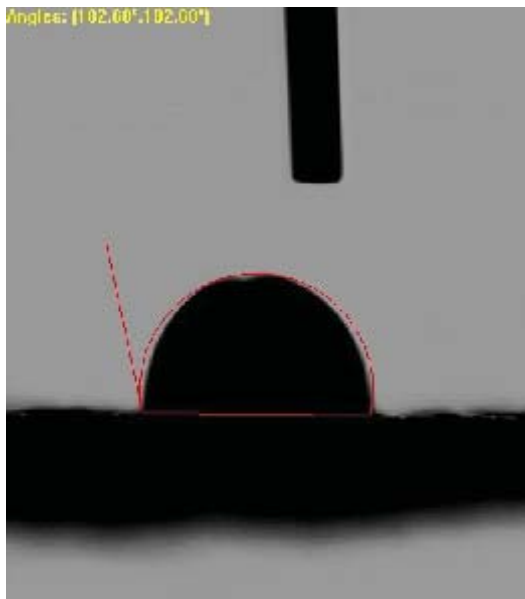


Figure 22h—The contact angle measurement of DI Water on the surface of the Nylon sample. The left and right contact angles are measured with the VCA Optima program. The left and right angles were both 102.60° .

Table IX— The measured contact angles for the Glass sample for all the solutions. Three measurements per solution were taken for better accuracy and the average was calculated for the Zisman plot

Glass		
Solution	Left	Right
70% Ethanol	20.3	20.3
	26.1	26.1
	24.8	24.8
Average	23.73333333	23.73333333
Methyl Salicyate	25.4	25.4
	29.6	26.7
	19.8	19.8
Average	24.93333333	23.96666666
DI Water	50.1	49.1
	47.8	47.6
	51.4	50.5
Average	49.76666667	49.06666666
Diethylene Glycol	32.5	32.5
	29.9	29.9
	29.5	29.5
Average	30.63333333	30.63333333

Table X— The measured contact angles for the Titanium sample for all the solutions. Three measurements per solution were taken for better accuracy and the average was calculated for the Zisman plot. There was only one attainable measurement for the Methyl Salicylate. Even though the droplet size was doubled to 1.5 μ L, the droplet evaporated too quickly for a snapshot to be taken with the VCA Optima program

Titanium		
Solution	Left	Right
70% Ethanol	44	44
	46.3	47.9
	44	44
Average	44.76666667	45.3
Methyl Salicylate	6.7	6.7
	*used 1.5microliter drops	
DI Water	97.2	97.2
	93.8	92.9
	77.3	76
Average	89.43333333	88.7
Diethylene Glycol	71	71
	66	66
	69.2	69.2
Average	68.73333333	68.73333333

Table XI— The measured contact angles for the Nylon sample for all the solutions. Three measurements per solution were taken for better accuracy and the average was calculated for the Zisman plot.

Nylon		
Solution	Left	Right
70%	70.8	72.2
	74.7	78.8
	81.1	82.9
Average	75.53333333	77.96666667
MS	92.2	91.5
	86.1	84.4
	108.2	108.5
Average	95.5	94.8
DI	80.5	82.9
	86.2	89.2
	93.2	94.2
Average	86.63333333	88.76666667
DIG	104.6	104.6
	98.5	98.5
	101.5	101.5
Average	101.5333333	101.5333333

B. Zisman Plot

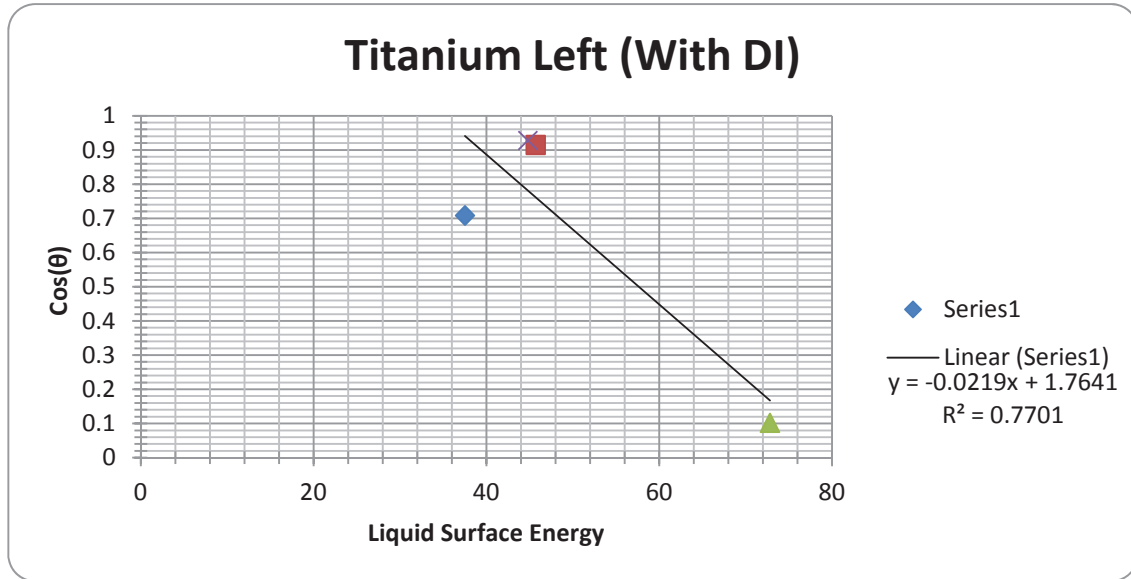
After the contact angles are tabulated in excel, I took the cosine of the average of both the left and right angles for all the solution and material combinations. (Table XII) Next I created a scatter plot with the cosine left angle values of each liquid plotted on the Y-axis and the surface energy of each solution is plotted on the X-axis. (Table XIII) I made sure that the cosine value of the 70% Ethanol was plotted against the surface energy 70% ethanol; I matched the remaining materials with their corresponding solutions. Next I added a linear trendline to the scatter plot, and included the equation of the line and the R^2 value. (Plot 1-6) I then set the equation of the line equal to 1 and solve for X – this produced the critical surface energy of the sample material.

Table XII— The Cosine(θ) values of the calculated average left and right contact angle values from the three samples.

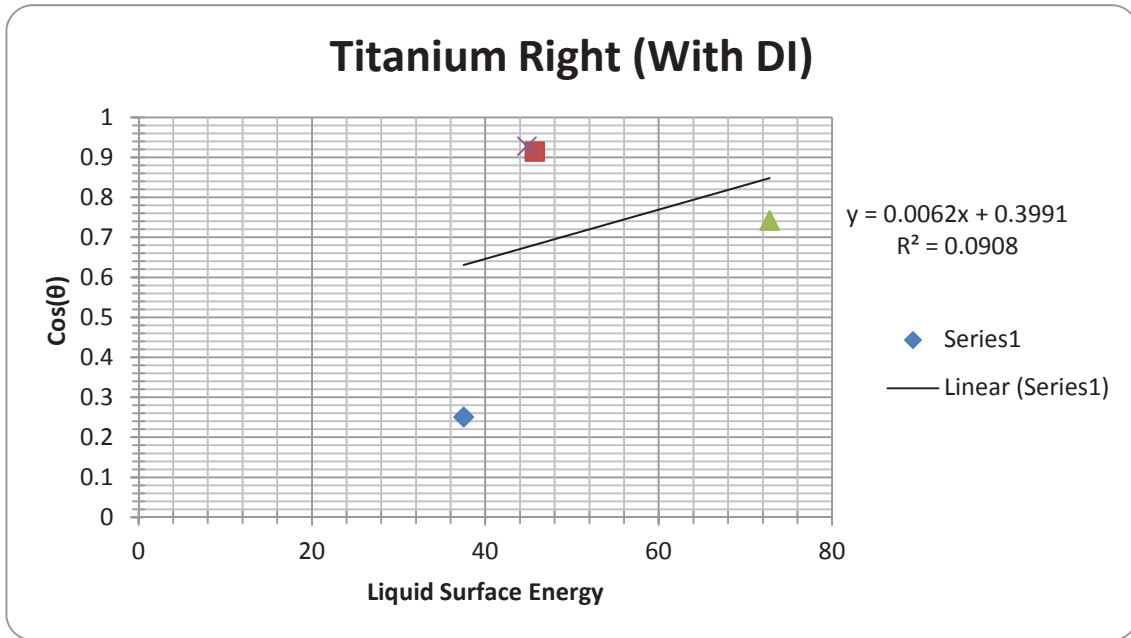
	Titanium		Glass		Nylon	
	Left	Right	Left	Right	Left	Right
70% Ethanol	0.707834	0.2504	0.170550602	0.170550602	0.990886568	- 0.840197137
Methyl Salicylate	0.914383	0.914383	0.980184039	0.393763018	0.313214469	0.851361851
DI Water	0.10188	0.741559	0.878149687	0.363461229	0.237251278	0.69521859
Diethylene Glycol	0.928031	0.928031	0.709087404	0.709087404	0.538307837	0.538307837

Table XIII— The given surface energies for Methyl Salicylate, DI Water, and Diethylene Glycol, the liquids used for the contact angle measurements. The surface energy of 70% Ethanol was calculated using Equation 4.

Liquid Surface Energies	
70% Ethanol	37.52
Methyl Salicylate	45.7
DI Water	72.8
Diethylene Glycol	44.8

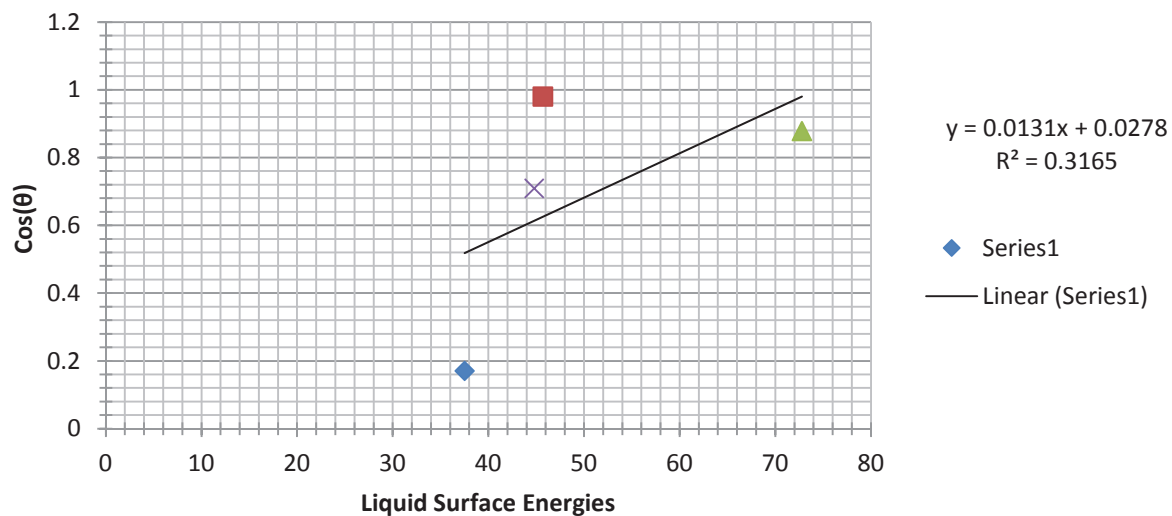


Plot 1— Zisman plot of the measured left contact angles for Titanium. The $\cos(\theta)$ values of the measured contact angles are plotted on the X-axis, while the liquid surface energies of the solutions are plotted on the Y-axis. The DI Water X and Y data points are plotted. The critical surface energy is computed by setting the equation for the linear trend line equal to 1 and solving for X.



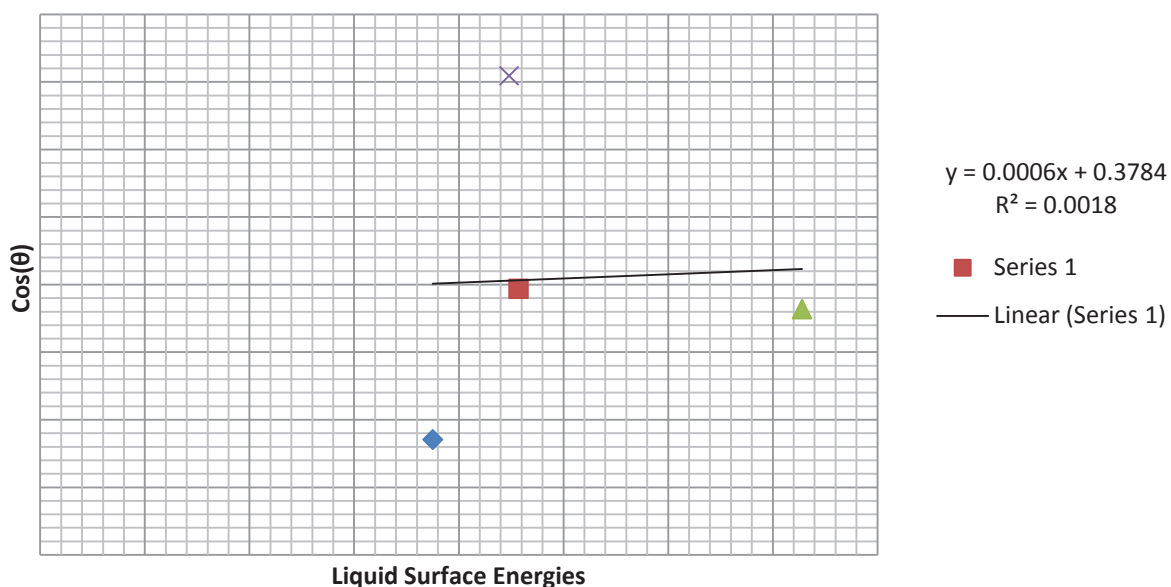
Plot 2— Zisman plot of the measured right contact angles for Titanium. The $\cos(\theta)$ values of the measured contact angles are plotted on the X-axis, while the liquid surface energies of the solutions are plotted on the Y-axis. The DI Water X and Y data points are plotted. The critical surface energy is computed by setting the equation for the linear trend line equal to 1 and solving for X.

Glass Zisman Left (With DI)

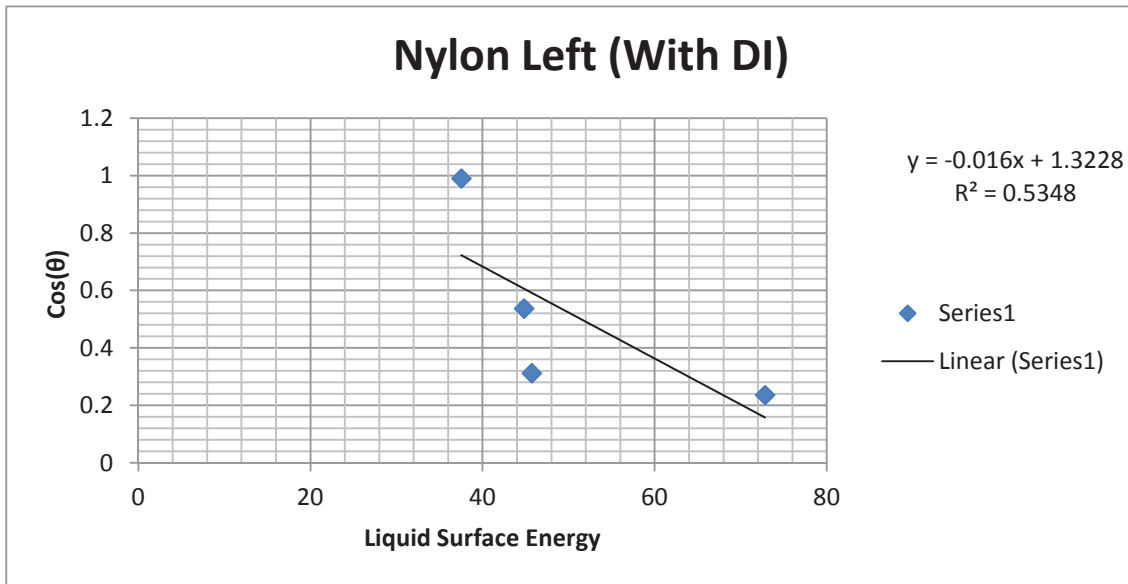


Plot 3— Zisman plot of the measured left contact angles for Glass. The Cos(θ) values of the measured contact angles are plotted on the X-axis, while the liquid surface energies of the solutions are plotted on the Y-axis. The DI Water X and Y data points are plotted. The critical surface energy is computed by setting the equation for the linear trend line equal to 1 and solving for X.

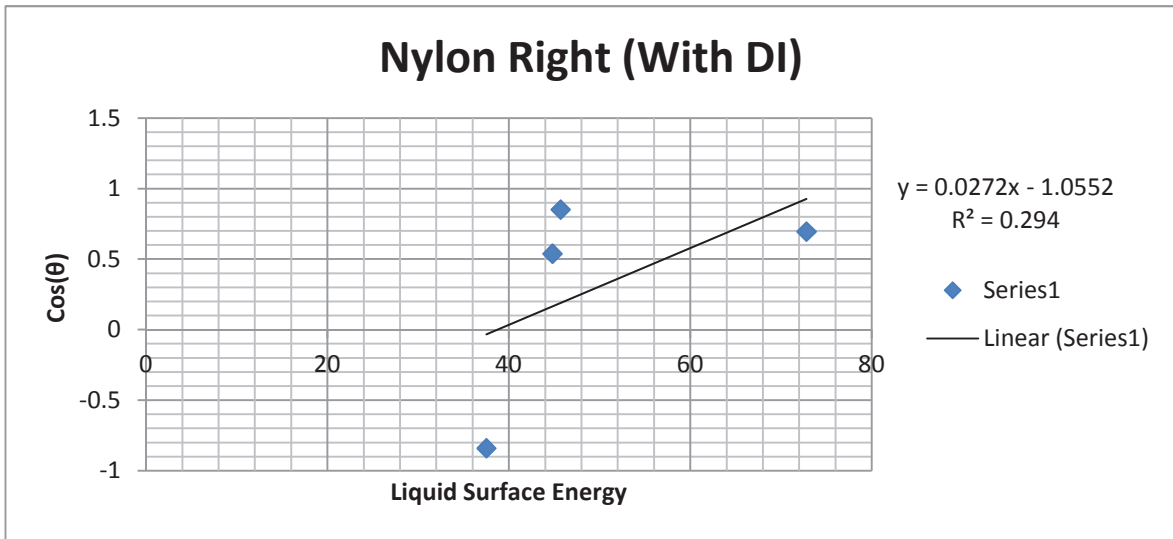
Glass Zisman Right (With DI)



Plot 4— Zisman plot of the measured right contact angles for Glass. The Cos(θ) values of the measured contact angles are plotted on the X-axis, while the liquid surface energies of the solutions are plotted on the Y-axis. The DI Water X and Y data points are plotted. The critical surface energy is computed by setting the equation for the linear trend line equal to 1 and solving for X.



Plot 5— Zisman plot of the measured left contact angles for Nylon. The $\text{Cos}(\theta)$ values of the measured contact angles are plotted on the X-axis, while the liquid surface energies of the solutions are plotted on the Y-axis. The DI Water X and Y data points are plotted. The critical surface energy is computed by setting the equation for the linear trend line equal to 1 and solving for X.



Plot 6— Zisman plot of the measured left contact angles for Nylon. The $\text{Cos}(\theta)$ values of the measured contact angles are plotted on the X-axis, while the liquid surface energies of the solutions are plotted on the Y-axis. The DI Water X and Y data points are plotted. The critical surface energy is computed by setting the equation for the linear trend line equal to 1 and solving for X.

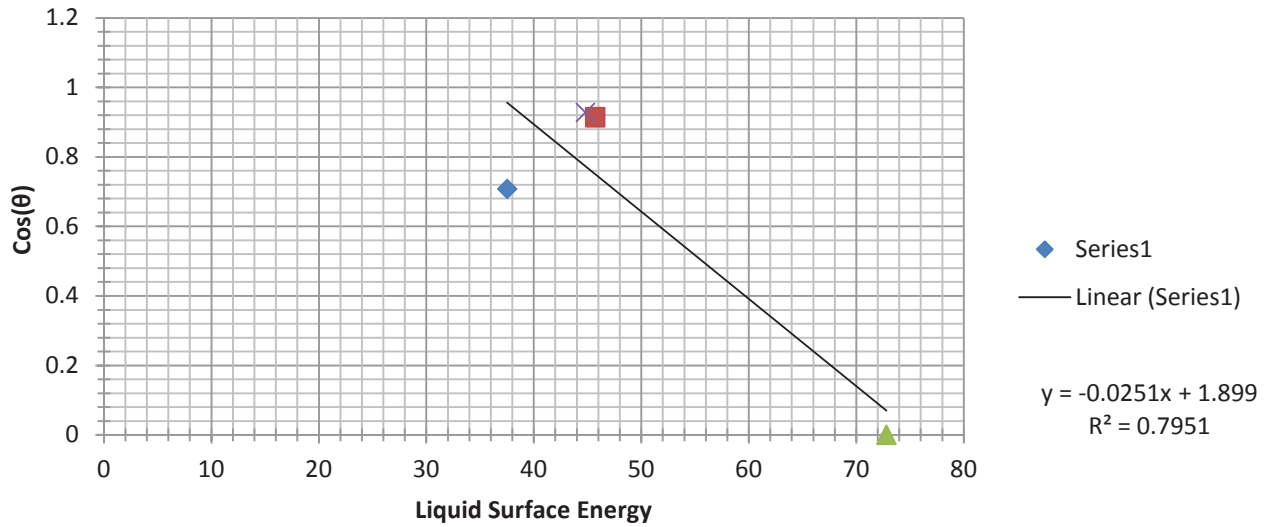
3.3 RESULTS

Calculating the critical surface energies for Titanium, Glass, and Nylon was done with the use of the Zisman plots. The critical surface energy for Titanium obtained from the left and right contact angles were 34.89 and 96.92 dynes/cm respectively. The Glass critical surface energies obtained from the left and right contact angles were 74.9 and 1036 dynes/cm respectively. The Nylon critical surface energies were 20.175 and 75.56 dynes/cm for the left and right contact angles respectively. (Table XIV) However, it appeared to me that the DI Water data point was consistently the outlier; I believed this was the reason that the experimental critical surface energies were not matching up with the literature values. Thus I created Zisman plots without the DI Water data points for each material; I graphed the surface energy of the DI Water on the X-axis, but not the corresponding Cos(θ) value on the Y-axis. The linear trendlines without the DI Water data point showed an increase in the R² value compared to the previously mentioned Zisman plots. (Plot 7-12).

Table XIV— Calculated surface energies of Titanium, Glass, and Nylon; values were computed using the Zisman plots with and without the DI Water data point. Because there are left and right contact angle measurements, the surface energies were calculated with both sets of data

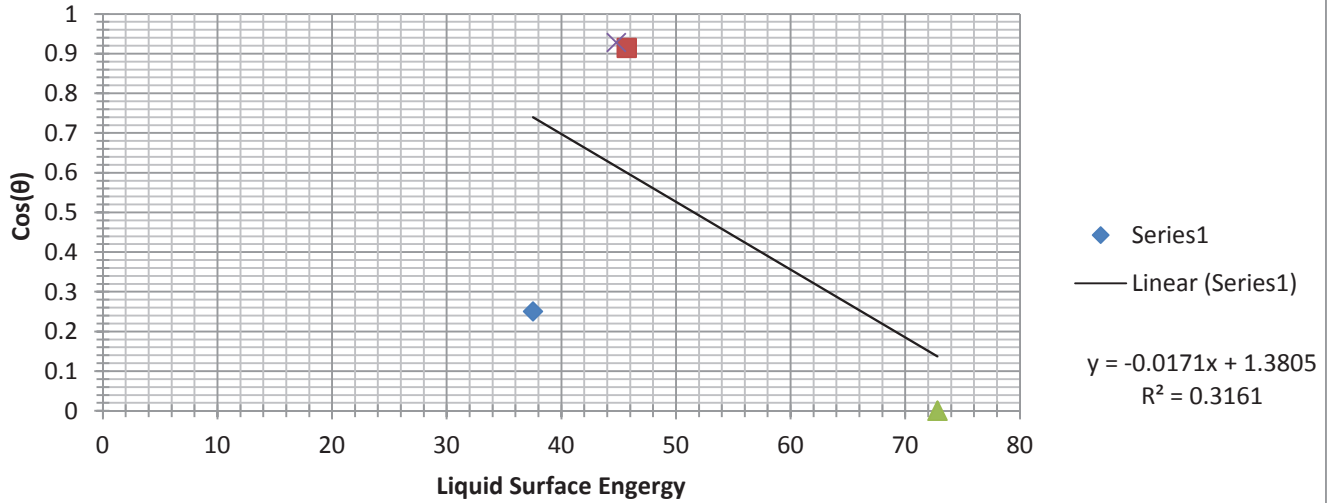
	Surface Energy With DI Data Point		Surface Energy Without DI Data Point	
	Left	Right	Left	Right
Titanium	34.89	96.92	48.14	35.52
Glass	74.9	1036	46.90	55.33
Nylon	20.175	75.56	37.5	46.75

Titanium Left (No DI)



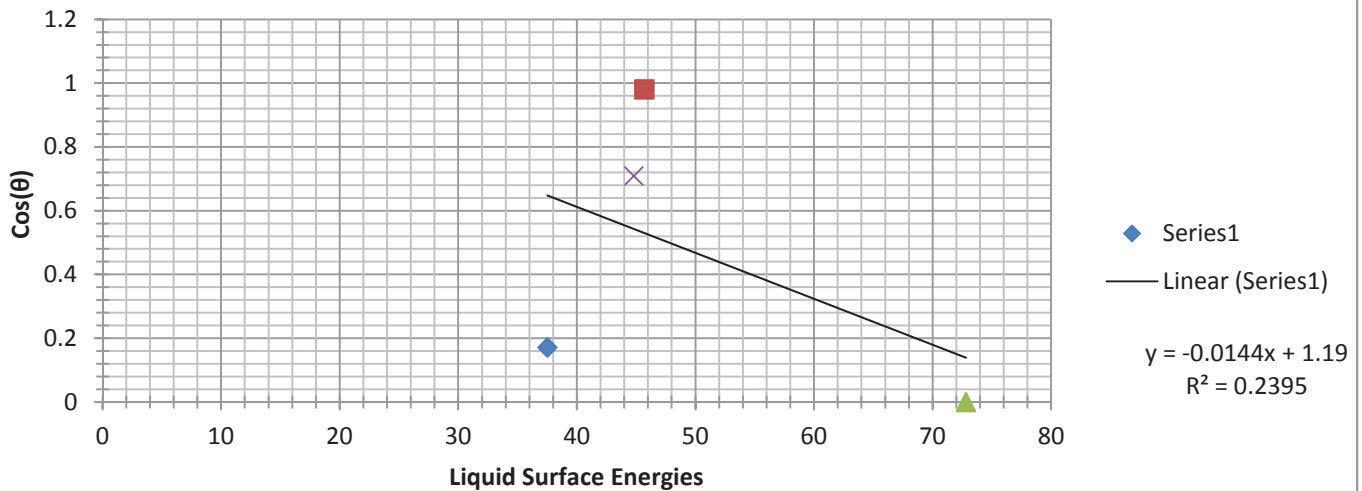
Plot 7— Zisman plot of the measured left contact angles for Titanium. The $\text{Cos}(\theta)$ values of the measured contact angles are plotted on the X-axis, while the liquid surface energies of the solutions are plotted on the Y-axis. The DI Water Y data point is not plotted, while the X data point is The critical surface energy is computed by setting the equation for the linear trend line equal to 1 and solving for X.

Titanium Right (No DI)



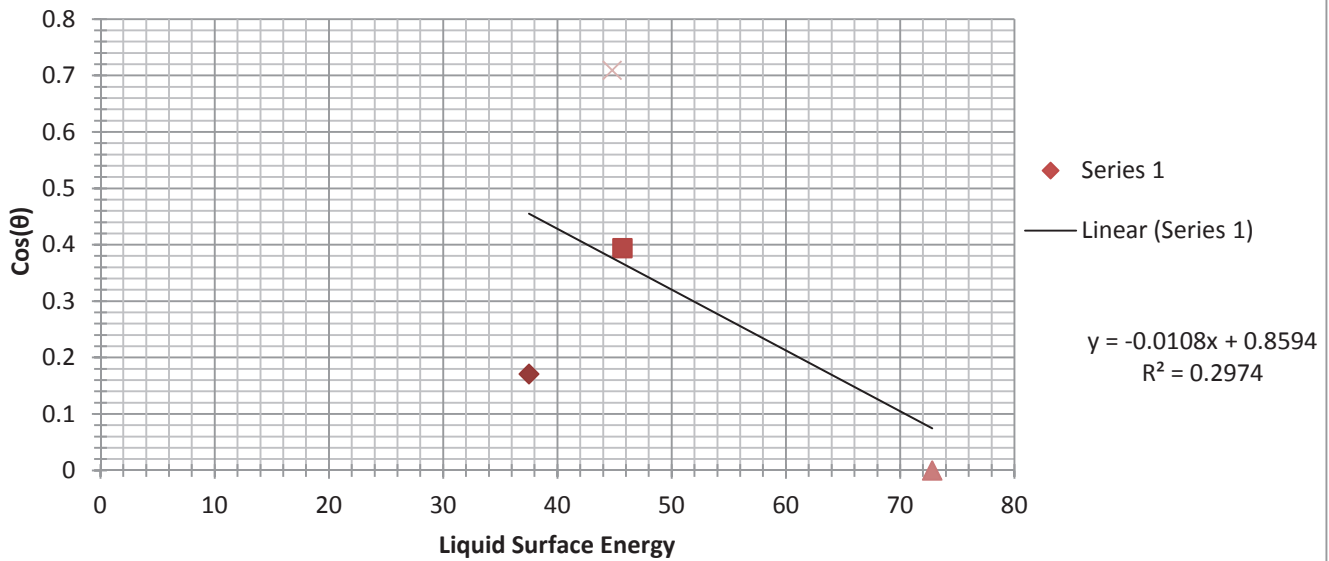
Plot 8— Zisman plot of the measured right contact angles for Titanium. The $\text{Cos}(\theta)$ values of the measured contact angles are plotted on the X-axis, while the liquid surface energies of the solutions are plotted on the Y-axis. The DI Water Y data point is not plotted, while the X data point is The critical surface energy is computed by setting the equation for the linear trend line equal to 1 and solving for X.

Glass Zisman Left (No DI)



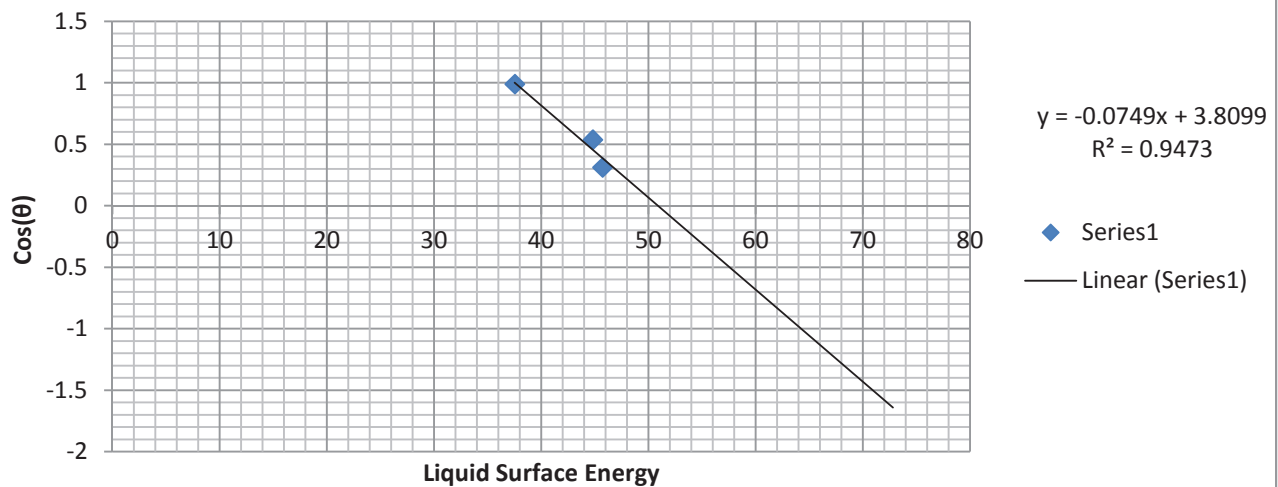
Plot 9— Zisman plot of the measured left contact angles for Glass. The $\text{Cos}(\theta)$ values of the measured contact angles are plotted on the X-axis, while the liquid surface energies of the solutions are plotted on the Y-axis. The DI Water Y data point is not plotted, while the X data point is The critical surface energy is computed by setting the equation for the linear trend line equal to 1 and solving for X.

Glass Zisman Right (No DI)

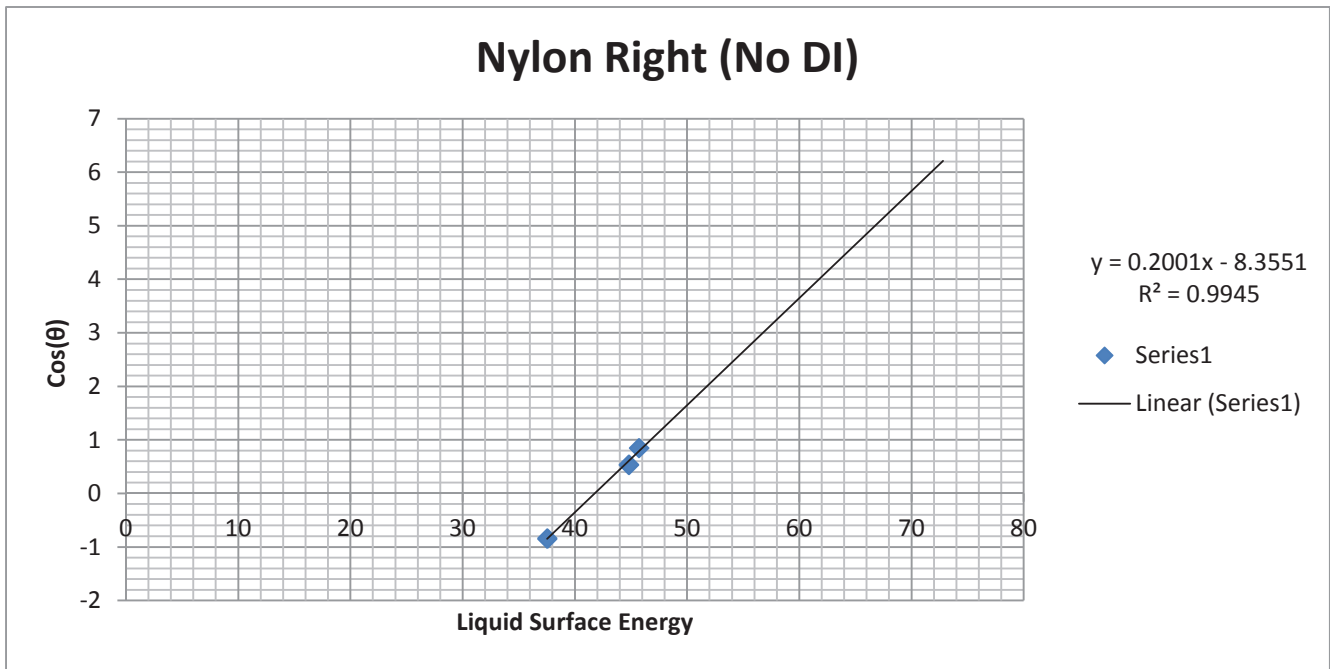


Plot 10— Zisman plot of the measured right contact angles for Glass. The $\cos(\theta)$ values of the measured contact angles are plotted on the X-axis, while the liquid surface energies of the solutions are plotted on the Y-axis. The DI Water Y data point is not plotted, while the X data point is The critical surface energy is computed by setting the equation for the linear trend line equal to 1 and solving for X.

Nylon Left (No DI)



Plot 11— Zisman plot of the measured left contact angles for Nylon. The $\cos(\theta)$ values of the measured contact angles are plotted on the X-axis, while the liquid surface energies of the solutions are plotted on the Y-axis. The DI Water Y data point is not plotted, while the X data point is The critical surface energy is computed by setting the equation for the linear trend line equal to 1 and solving for X.



Plot 12— Zisman plot of the measured right contact angles for Nylon. The $\text{Cos}(\theta)$ values of the measured contact angles are plotted on the X-axis, while the liquid surface energies of the solutions are plotted on the Y-axis. The DI Water Y data point is not plotted, while the X data point is The critical surface energy is computed by setting the equation for the linear trend line equal to 1 and solving for X.

3.4 DISCUSSION

The literature values for the surface energies of Titanium, Glass, and Nylon are 20-30, 47, and 33 dynes/cm respectively. Although I did not obtain the literature surface energies, I was able to come close. I did discover a trend with eliminating the DI Water y-coordinate of each plot; when the DI water y-coordinate is eliminated, but the DI Water x-coordinate was left alone, the experimental surface energies were closer to the literature values, and the linear trend lines increased greatly in correlation which can be observed by taking note of the increase in R^2 value of the linear trendlines. I eliminated the DI water data point (Y-axis coordinate but not the X-axis coordinate) because it was most obvious outlier because of its high surface energy value, however I still believe that the DI water should be included in the contact angle lab.

No lab experiment is perfect, and for this procedure there are plenty of factors that could have led to inaccurate data. The titanium was a scrap piece that BMED Tech David Laiho found for me, this means that the titanium sample could have well been exposed to an environment that might have contaminated its surface. Another factor of error is how the Figures are taken from only one perspective and allow room for noise. For example, when 70% Ethanol creates a droplet on the surface of the Titanium and Glass samples, it is clear where the edges of the liquid-solid interface are. Thus, placing the left and right angle markers for the contact measurements was easy and produced accurate results. (Figure 23a-23b) However, with Nylon, the surface of the sample is not completely flat and interferes with the users' ability to clearly identify where the left and right edges of the droplet are. Because the location of the liquid-solid interface is not clearly defined on the Nylon surface, the results can be skewed even when the Auto-Calculate function is used.

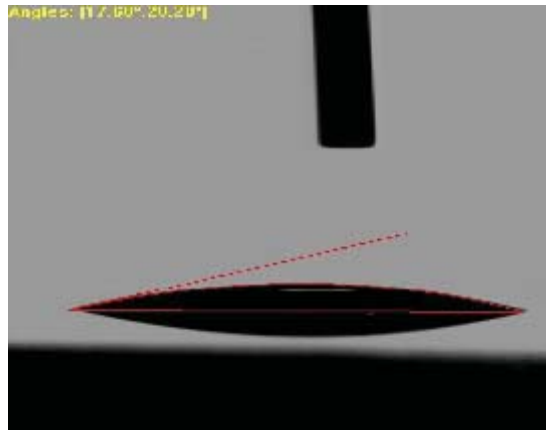


Figure 23a— Contact angle measurement for Glass. The edges of the liquid-solid interface are easily discernable, thus allowing for easy and accurate placement of the left and right angle markers.

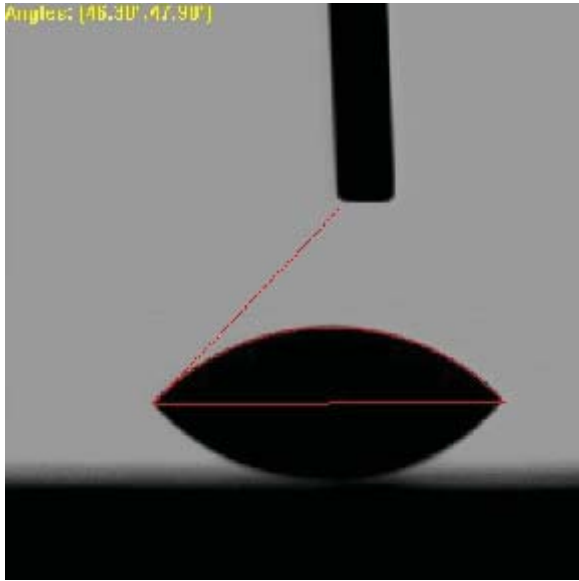


Figure 23b— Contact angle measurement for Titanium. The edges of the liquid-solid interface are easily discernable, thus allowing for easy and accurate placement of the left and right angle markers.

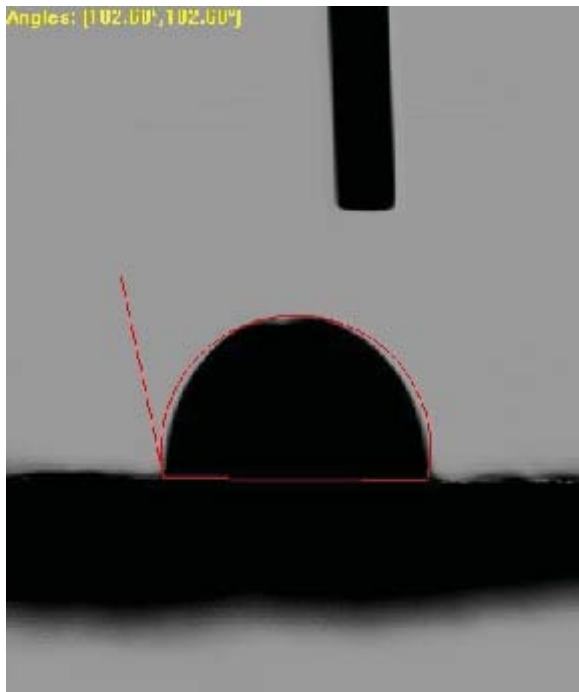


Figure 23a— Contact angle measurement for Nylon. The edges of the liquid-solid interface are difficult to identify, thus creating inaccurate placement of the left and right angle markers and inaccurate measurements.

To reiterate my objective for this portion of my senior project, I aimed to expand the contact angle lab by testing materials and determining whether or not they should be included in the lab. I believe that despite the fact that the experimental data does not exactly match up with the literature values titanium and glass should be added to the list of materials tested during the contact angle lab. However, I strongly believe that nylon should not be used for the contact angle lab because nylon tends to fray when it is cut into pieces, and this fraying behavior causes a lot of noise and interference with the VCA Optima program, thus producing inaccurate Figures and data.

4. Conclusion

The goal of my senior project was to have an impactful improvement on Lab B – Contact Angle and Lab F – Ultrasonic Biomaterial Analysis. For the Contact Angle lab, I tested three new potential materials – Glass, Titanium, and Nylon. The enhancement of the Ultrasound lab was done by creating bone samples that have a more cubic shape. This ensured that the send/receive configuration of the ultrasound testing would be used more efficiently. The elastic modulus of the new bone samples were slightly out of the literature value range, but that can be attributed to a number of factors. The biggest factor is the testing difference between the Lab F ultrasound tests performed by the students and the ultrasound tests performed by Grimal et. al. Although one of my secondary objectives for Lab F was to design and machine a new bone holding apparatus, the new bone samples are all relatively cubic and work exceptionally well with the original bone holding apparatus. The addition of 12 more reliable bone samples will prove to be a beneficial addition to the Ultrasound lab, as will documentation of the method for creating new samples

Using the literature material surface energy values as guidelines I performed the contact angle tests on the three materials. Despite not being able to attain the exact values literature values, the Titanium and Glass contact angle tests produced nice data and would serve to be useful additions to the current material list. Unfortunately, because of the surface roughness of the Nylon fabric the contact angle tests contain too much noise for the data to be of any value.

Ultrasonic testing and Contact angle measurements are prevalent in various principles of engineering. The way BMED 420 lab utilizes these two methods of testing is accurate and relevant to their use in the industry today.

Along with measuring the wettability of the surface of a material, contact angle measurement procedures are also being utilized to measure the hydrophobicity of water repellent soils, and the corrosion resistance of metallic glasses. Beatty et. al. use contact angle measurements to analyze the behavior of fire affected soils 1.5 years post fire; the authors used contact angle measurements to deduce that the hydrophobicity of the soils was due to the changes in the surface properties of the soils and not the surface tension of the fluid trying to wet the soil (Beatty and Smith, Fractional wettability and contact angle dynamics in burned water repellent soils."). Nguyen et. al. used contact angle measurements to test the repellency of a new superomniphobic surface composed of silicon nanowires; the authors dropped diiodomethane onto their nanowire surface and studied how the behavior and contact angle formed upon impact onto the material (Nguyen et. al., "Quantitative Testing of Robustness on Superomniphobic Surfaces by Drop Impact.").

Ultrasonic testing is currently being used for bone analysis and material analysis because of its noninvasive nature. Muller et. al. used ultrasonic testing to send waves to analyze the microdamages that occur in humans from daily cyclic loading; the authors placed their bone samples under fatigue testing to simulate cyclic loading, and the ultrasonic testing was responsible for identifying the location and size of the damage within the bone (Muller et. al. "Nonlinear Ultrasound Can Detect Accumulated Damage in Human Bone."). Wu et. al. applied the nondestructive nature of ultrasound testing to compute the mechanical properties of metal; instead of using sound waves, the authors sent a laser beam to the metal sample which was then converted to ultrasonic signals and analyzed (Wu et. al. "Integrated Piezoelectric Ultrasonic Receivers for Laser Ultrasound in Non-destructive Testing of Metals).

Within the scope of the BMED 420 lab, the tools and methods being utilized by the students are great supplemental materials for reinforcing the BMED 420 lecture. The relevance of both the Ultrasound lab and the Contact Angle lab to their uses in the industry produces a hope for students that what they're learning can be applied to their career. As technology evolves and our knowledge of the science of biomaterials increases, the labs will have to be updated with their use within the industry. In the future, the Ultrasound lab and the Contact Angle lab can be used with the same procedures but with a different goal.

5. References

- Grimal, Quentin , Laurent Vastel, Sylvain Hauptert, Pascal Laugie, and David Mitton. "Assessment of Cortical Bone Elasticity and Strength: Mechanical Testing and Ultrasound Provide Complementary Data." *Medical Engineering and Physics* 31.9 (2009): 1140-1147. *Engineering Village 2*. Web. 13 Sept. 2011.
- "Introduction to Ultrasonic Testing." *NDT Resource Center*. NDT, n.d. Web. 13 Sept. 2011. <<http://www.ndt-ed.org/EducationResources/CommunityCollege/Ultrasonics/Introduction/description.htm>>.
- Menzies, Kara , and Lyndon Jones. "The Impact of Contact Angle on the Biocompatibility of Biomaterials." *Optometry and Vision Science* 87.6 (2010): 387-399. *Engineering Village 2*. Web. 13 Sept. 2011.
- Muller, M , P Johnson, D Mitton, P Laugier, and M Talmart. "Nonlinear Ultrasound Can Detect Accumulated Damage in Human Bone." *Journal of Biomechanics* 41.5 (2008): 1062-1068. Print.
- "Normal Beam Inspection." *NDT Resource Center*. NDT, n.d. Web. 13 Sept. 2011. <<http://www.ndt-ed.org/EducationResources/CommunityCollege/Ultrasonics/MeasurementTech/beaminspection.htm>>.
- Pithioux, M, and P Lasaygues. "Ultrasonic Characterization of Orthotropic Elastic Bovine Bones." *Ultrasonics* 8.39 (2002): 567-573. *Engineering Village 2*. Web. 13 Sept. 2011.
- Wu , K. -T , A Blouin, C.-K Jen, and M Kobayashi. "Integrated Piezoelectric Ultrasonic Receivers for Laser Ultrasound in Non-destructive Testing of Metals." *Journal of Nondestructive Evaluation* 30.1 (2011): 1-8. Print.
- BMED 420 - Lecture and Lab - Winter 2011
- Beatty, Sarah M., and James E. Smith. " Fractional wettability and contact angle dynamics in burned water repellent soils." *Journal of Hydrology* 391 (2010): 97-108. *Science Direct*. Web. 19 Sept. 2011.
- Nguyen, Thi Phuong Nhung, Philippe Brunet, Yannick Coffinier, and Rabah Boukherroub. "Quantitative Testing of Robustness on Superomniphobic Surfaces by Drop Impact." *American Chemical Society Journals* 26.23 (2010): 18369 -18373. *American Chemical Society*. Web. 18 Sept. 2011.
- Wang, Y. B. , H.F. Li, Y.F. Zheng, S.C. Wei, and M Li.. "Correlation between corrosion performance and surface wettability in ZrTiCuNiBe bulk metallic glasses." *Applied Physics Letters* 96.25 (2010): 251909. *APPLIED*

PHYSICS LETTERS. Web. 19 Sept. 2011.

Wu, K.-T., A. Blouin, C.-K. Jen, and M. Kobayashi. "Integrated Piezoelectric Ultrasonic Receivers for Laser Ultrasound in Non-destructive Testing of Metals." *Journal of Nondestructive Evaluation* 30.1 (2011): 1-8. Web. 19 Sept. 2011.

Deganello, D., T.N. Croft, A.J. Williams, A.S. Lubansky, D.T. Gethin, and T.C. Claypole. "Numerical simulation of dynamic contact angle using a force based formulation." *Journal of Non-Newtonian Fluid Mechanics* 166.16 (2011): 900-907. *Science Direct*. Web. 19 Sept. 2011.

C_{3,3}

One-way ANOVA: C7 versus C1

Source	DF	SS	MS	F	P
C1	3	62.7	20.9	1.57	0.271
Error	8	106.4	13.3		
Total	11	169.1			

S = 3.647 R-Sq = 37.08% R-Sq(adj) = 13.48%

Individual 95% CIs For Mean Based on Pooled StDev

Level	N	Mean	StDev	
L1	3	28.976	0.829	(-----*-----)
L2	3	24.179	5.011	(-----*-----)
L3	3	30.323	2.141	(-----*-----)
L4	3	27.596	4.778	(-----*-----)

-----+-----+-----+-----
20.0 24.0 28.0 32.0

Pooled StDev = 3.647

APPENDIX B

The laboratory protocol for Lab B – Contact Angle Measurement

LAB B: CONTACT ANGLE MEASUREMENT

BMED 420

PURPOSE OF THIS LAB EXERCISE

In this lab, you will measure various contact angles of a selection of liquids on polymeric materials in order to estimate the critical surface energy using a Zisman plot. The goal of this lab is to help you understand how critical surface energies differ among biomaterials and the reason for these differences.

INTRODUCTION

WHAT IS CONTACT ANGLE?

The contact angle is the angle between a liquid-vapor interface and the solid surface it is interfacing with. This can also form between two liquids or two vapors interfacing on a solid surface. The shape of the droplet can be modeled by the Young-Laplace equation. Figure 1 shows an example of the contact angle, θ_c , that the droplet makes with the surface.

The contact angle, and subsequently the shape of the droplet, is determined by the difference between the liquid-liquid and liquid-solid inter-molecular forces. These are forces of surface tension. If the difference is small, the contact angle will be very small, as the droplet will try to spread out over a large surface area. If the difference is large, the contact angle will be much higher, approaching 90 degrees. In the case of water, if the surface is hydrophobic, the contact angle surpasses 90 degrees and may approach 180 degrees. In this case there is almost no actual contact with the droplet and the surface. This results from thermodynamic equilibrium in which the chemical potential of all phases present are equal. Figure 2 shows examples of a water droplet's shape on hydrophobic and hydrophilic surfaces.

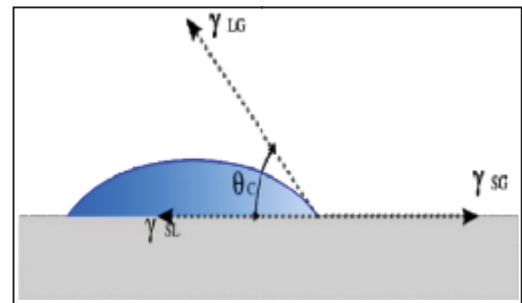


Figure 1 - The angle between the surface and droplet is termed the contact angle (θ_c).

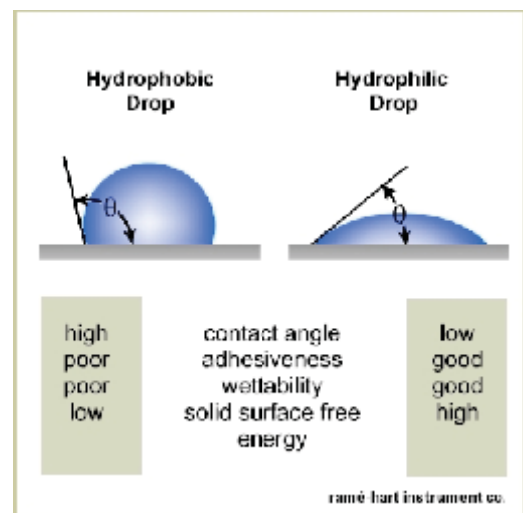


Figure 2 - Hydrophobic and Hydrophilic Contact Angles. Hydrophobic drops have large contact angles, while Hydrophilic drops have very small contact angles

HOW IS THE CONTACT ANGLE MEASURED?

Using the equations and concepts mentioned above, machines such as the VCA Optima system use microscopic side imaging to create a high-contrast image of droplets of liquid on a given surface, which can then be easily quantified using computer measurement systems. An example of such an image is shown in Figure 3. These images are to be analyzed just as the drawings above.

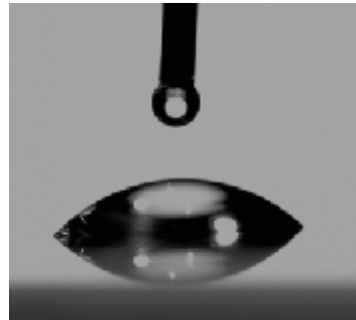


Figure 3 – A high-contrast image of a contact angle

WHY IS THE CONTACT ANGLE IMPORTANT?

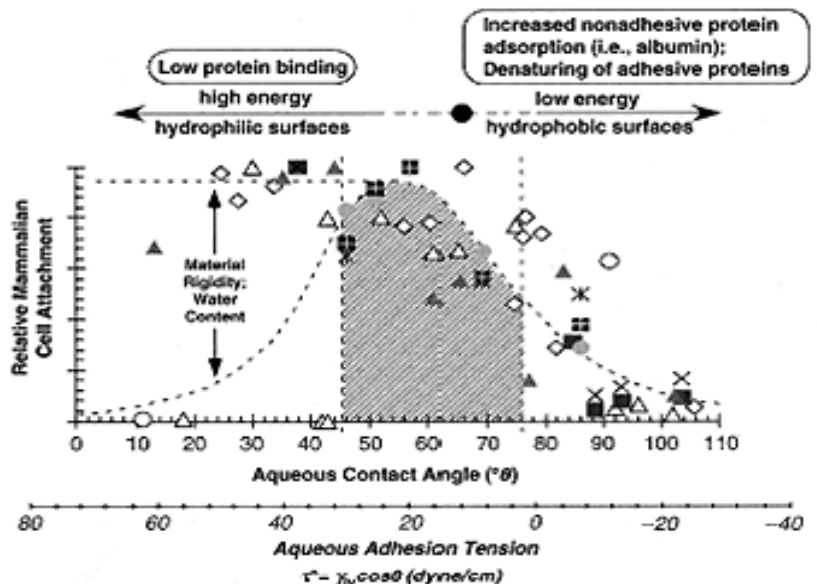
The contact angle can affect the wettability and tissue adhesion of a material. These are both important attributes for a biomaterial, as they affect how the body interacts with the material. When selecting materials for use in a bioreactor or tissue engineered construct, contact angle measurement devices allow the user to easily predict likely *in-vivo* and *in-vitro* characteristics of the surface. Figure 4 indicates that polymeric materials typically have optimal surface energy/contact angle for cell attachment.

POROSITY AND CONTACT ANGLE

As mentioned before, surface energy correlates with cell attachment— however, the material’s surface properties such as those involving the material’s porosity and tendency towards interfacial hydration can also impact cell attachment. As porosity affects cell attachment, it also affects the surface energy of the material, creating a difference that is measurable with contact angle systems.

SURFACE ENERGY AND CONTACT ANGLE

To prevent dissolution in water, polymers with high surface energies (low contact angles) are typically cross-linked to form hydrogels. These gels tend to absorb water: the matrix swells, the mechanical modulus lowers, and the surface elasticity increases. Cells will have difficulty attaching to this matrix. This phenomenon can be seen on the left side of Figure 4. Likewise, low surface energy levels (high contact angles) display similar low cell-attachment. The optimal cell culture surface is found between these two states,



typically around 65° .

Figure 4 - The above figure is a plot of contact angle versus cell attachment. The plot demonstrates that prime cell attachment occurs between 45° and 75° .



Molecules of a material located on the surface are at a higher energy state compared to those located inside a solid body. This phenomenon is the reason why creating surfaces or cutting a solid into pieces requires energy. Since molecules on the inside of a material exist at a lower energy state, the number of molecules located on the surface is minimized at any given time. Intermolecular forces and interactions between cohesion and adhesion determine the shape of a bead of liquid.

METHODS

EQUIPMENT


- Contact angle measurement system
- Powderless gloves
- Material Samples (Silicone and Copper)

LIQUIDS USED FOR TESTING

- DI Water
- Methyl Salicate
- Diethylene Glycol
- Ethanol



TESTING METHODS - PROTOCOL

PART ONE: USING VCA-OPTIMA TO OBTAIN MEASUREMENTS

1. Turn on the equipment-- the computer, and the measuring device (switch is on the back).
2. Put on gloves. *It is essential that all materials stay sterile and uncontaminated throughout this lab.* Even the oils from your hands can skew your results.
3. Check to make sure that the testing machine is level by looking at the alignment bubble and adjusting the feet. Check that the syringes are full. It should contain enough liquid to perform the experiment ($>1 \mu\text{L}$). If it does not, contact your lab tech or instructor for assistance.
4. Attach your samples to a glass slide with double-sided tape. When handling the sample, try to only touch the glass. *Keep all liquids and materials as clean as possible throughout the lab.*
5. Ensure that the top surface of the material is not touched as you place the sample on the stage of the testing machine.
6. Open VCA-Optima. If you have trouble connecting, make sure that the device board (inside the computer) is not loose, and that all cables are connected to the computer.
7. Raise the stage until it is visible on the screen. If the syringe is not visible at the top of the screen, ask your instructor for assistance.
8. Click on the  button. Under “droplet,” make sure that the size is $0.75\mu\text{L}$, and that it is set to “dispense.” Click “Go” until a droplet forms. Do not worry if the droplet adheres to the side of the needle. Slowly (**VERY slowly**).



You do not want to add energy to the system) raise the tray until the drop meets your sample, and lower it to detach the droplet.

9. Wait approximately 3 seconds, or until the liquid has ceased to visibly shift. Click  to take a snapshot.
10. Auto-calculate the contact angle of the droplet by clicking . If the measurement is inaccurate, you can manually arrange the letters/numbers around the droplet: (clockwise starting at the left edge of the drop) **L** (left), **T** (top), **R** (right) (**1** and **2** are not necessary). If you still have problems taking a measurement, make sure the backlight is off, or have someone stand in front of the device to darken the droplet. You might also need to click the “low angle” button if the droplet is very spread out.
11. Record the measurements and their corresponding liquids in Excel. Record both the left and right angle measurements. You will use them as if they are two different measurements.
12. It is not necessary to clean each sample between measurements—however, you will want to keep enough space between droplets such that they will not interfere with other measurements.
13. Shut down all equipment, including computers, and clean up materials after use.
14. Consult Table 2 for the specific surface energies associated with each liquid.
NOTE: Some liquids may require a ‘rule of mixtures’ calculation to obtain surface energy.

$$\gamma_{\text{mixture}} = V_{\text{fl}} \gamma_1 + (100 - V_{\text{fl}}) \gamma_2$$

Here, V_{fl} is the volume fraction of the 1st constituent, and γ_i is the surface energy of the liquids.

15. Create a Zisman Plot (Figure 5) in excel using your data. The y-axis will be the cosine of the particular liquid's contact angle, and the x-axis is the surface energy of that particular liquid. Add a linear trend line to the data (you should have two sets of data per material, and therefore two trend lines), and use the equation of the line to determine the surface energy of a zero degree ($\text{Cos}\theta = 1.0$) contact angle. Keep in mind that the y-axis corresponds to the cosine of the contact angle. This value is the critical surface energy of the material.
*****Note:** Excel uses *radians* for angles in trig functions and the VCA reports angles in degrees.
16. Compare measured critical surface energies to known values on Table 1 to verify correct values.

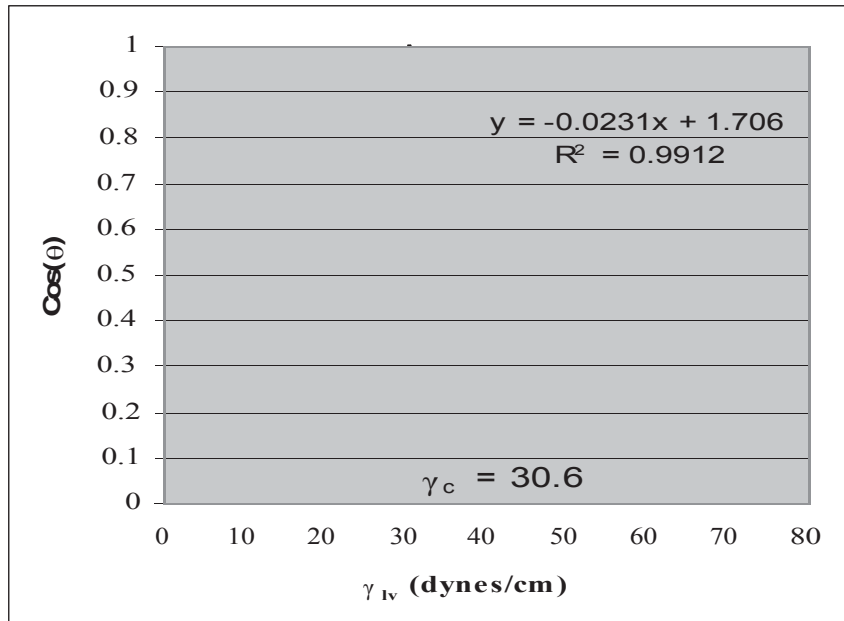


Figure 5 - A Zisman plot used to calculate the critical surface tension.

DISCUSSION QUESTIONS

1. What are possible sources of error? What are some ways to minimize these errors?
2. Which of the materials tested would be best for tissue growth? Explain.
3. How does contact angle correlate with surface energy?
4. Why must we use a sessile drop technique rather than let the drop fall from the syringe?
5. What are some other possible benefits of knowing a material's contact angle? Feel free to use peer-reviewed articles to help support your arguments (cite appropriately).
6. What are some other applications of contact angle testing /observation? For inspiration, check out the "electrowetting" technique perfected by the Duke microfluidics group: <http://microfluidics.ee.duke.edu/>

TABLE 1: MATERIAL SURFACE ENERGIES

Material	Surface Energy (dynes/cm)
Gore-tex (porous Polytetrafluoroethylene)	18-20
Titanium	20-30
Glass	47
316L Stainless Steel	35
Silicone rubber	22-24
High density polyethylene	30-31
Natural Rubber	24
Nylon	33
Copper	44
Polyacrylate	35
Polyimide	40

TABLE 2: LIQUID SURFACE ENERGIES

Liquid	Surface Energy (dynes/cm)
DI Water	72.8
Methyl Salicate	45.7
Diethylene Glycol	44.8
100% Ethanol	22.4

WORKS CITED

1. Guelcher, S. A, Hollinger, J. O; An Introduction to Biomaterials (2006) Cell-Material Interactions, Pgs 20-24
2. Hansen, F.K.; The measurement of surface energy of polymer by means of contact angles of liquids on solid surfaces (2004)
3. Ratner, B.D., et al; Biomaterials Science (2004) Contact Angle Methods, Pgs. 44-45

Fig. 1 Various Authors; *Contact Angle*;
http://commons.wikimedia.org/wiki/Image:Contact_angle.svg; Accessed 1/21/08

Fig. 2 Ramé-Hart Instrument Co.; *Contact Angle*;
<http://www.ramehart.com/goniometers/contactangle.htm>; Accessed 1/22/08

Fig. 3 Various Authors; *Contact Angle*; http://commons.wikimedia.org/wiki/Image:Video_contact_angle.gif; Accessed 1/22/08

Fig. 4 Guelcher, S. A, Hollinger, J. O; An Introduction to Biomaterials (2006) Cell-Material Interactions, Pg. 21

APPENDIX C

The laboratory protocol for Lab F – Ultrasonic Biomaterial Analysis

LAB F: ULTRASONIC BIOMATERIAL ANALYSIS

BMED 420

PURPOSE OF THIS LAB EXERCISE

The purpose of this lab is to compute the elastic modulus of bovine femur using ultrasonic analysis and to determine if there is any variance in the elastic modulus between the medial, lateral, cranial and caudal parts of the bone.

INTRODUCTION

The use of ultrasonic testing on biomaterials allows us to analyze material properties such as the elastic modulus, intrinsic flaws or physical measurement. Due to the non-invasive and non-destructive characteristics of ultrasonic testing it is appealing to the biomaterial field.

ULTRASOUND THEORY

The principle of ultrasonic testing uses echo location to analyze the material. Two different kinds of waveforms, longitudinal and shear, are used to detect material properties. These waveforms are transmitted at various frequencies ranging from 20 kHz to over 100 MHz with a working range from 500 kHz to 20 MHz. Shorter wavelengths are more responsive to changes in the medium through which they pass. Therefore, material analysis applications will benefit from using the highest frequency that the test piece will support. In the case of bone, 2.25 MHz is the most commonly used frequency [1]. Using pulse echo location, the wave velocities can be calculated through the material specimen. Basically, the time delay from when the wave is first transmitted to when the wave is received allows for detection and calculation of material properties [2].

Ultrasonic sound waves are produced by the conversion of an electrical pulse to a mechanical vibration and the conversion of the return mechanical vibrations back into electrical energy. This conversion takes place using a piezoelectric transducer. The frequency of a transducer depends primarily on the backing material. Highly damped transducers allow for a broad frequency range giving them high resolution. This high resolution allows defects near the surface of the material to be detected more easily. A less damped transducer will have a more narrow frequency range, which produces a poorer resolution but allows for greater penetration [3]. The signals from the transducers are processed through a computer and displayed.

ADVANTAGES OF ULTRASONIC ANALYSIS

Ultrasonic techniques offer advantages over mechanical testing for determining the elastic properties of biomaterials such as bone. The process is non-invasive, non-destructive and sensitive to surface and subsurface discontinuities [4]. Ultrasonic specimens can be smaller with a less complicated shape making specimen fabrication easier. Ultrasonic methods also allow the measurement of several anisotropic properties from one specimen. In the case of a biomaterial such as bone, which has inhomogeneity, anisotropy and limited size, these advantages are significant [5].

ORTHOPEDIC APPLICATIONS

When implanting an orthopedic device, it is important to know the mechanical properties needed for such a device so that the new biomaterial being used will function properly in the host. Using ultrasonic techniques, it is possible to measure certain parameters such as transit time, attenuation, frequency content and scattering. These can be correlated with physical properties such as hardness, density, elastic modulus, homogeneity and grain structure, all of which are important in deciding which type of material should be used in an orthopedic device with an expected life ranging from months to years [1].

The materials used for orthopedic implants are expected to function over a long period of time. They will be subjected to stresses and strains continuously for many years and thus need to have a specific set of physical properties so that they do not fail. Also, if the joint replacement is too stiff, problems such as bone loss (osteolysis) or fracture are more likely to occur around the joint.

Using ultrasonic techniques it is possible to measure these important properties for both bone and the implantable device. It is necessary to understand the mechanical properties of bone so that an implantable device can be manufactured with properties as similar as possible to the bone. Information obtained from ultrasonic analysis of bones is vital for biomedical companies that make orthopedic devices. Employees in research and development need this data to make the most reliable devices possible. Orthopedic surgeons rely on the fact that the implant they are using is made of the right type of material so that they can ensure their patients are receiving the best treatment possible.

Ultrasonic analysis can also be used as a form of quality control for not only orthopedic implants, but a wide variety of biomaterials. Using ultrasonic analysis, it is possible to find small defects, such as cracks within a material that might adversely affect its performance. It is critical to minimize this possibility when the materials are being used within the human body.

Ultrasonic analysis can be used as a simple, noninvasive way to measure the elastic properties of bone. It requires a sample of known dimensions and weight. From this it is possible to measure the speed of the ultrasonic waves through the bone and relate the elastic modulus to the density of the bone sample and the wave speed through the sample using equation 1.

$$C_{ij} = \rho v_{ij}^2 \quad [\text{Eq. 1}]$$

Here, ρ is the density, v is the wave velocity, C is the stiffness coefficient and the subscripts indicate tensor component.

METHODS

EQUIPMENT

- Micrometer Caliper
- Panametrics NDT
- Calibration sample
- Microbalance
- Graduated cylinder

MATERIALS

- Bone samples
- Mineral Oil (coupling agent)
- Water

TESTING METHODS - PROTOCOL

PART ONE: SAMPLE PREPARATION

1. Obtain required laboratory materials including prepared bone samples, Panametrics NDT, calipers and graduated cylinder partially filled with water.
2. Weigh all the samples of bone on the microbalance. Be organized, since there are several different samples. Record all values in the data tables at the end of this handout.
3. Calculate the apparent density of the bone by using the ratio between the mass and volume i.e. Archimedes Principle.
 - a. The volume will be determined with the use of a graduated cylinder. Fill partly with water. Record volume of water. Place sample into filled graduated cylinder. Record volume of water with added bone. The water displaced will indicate the volume. Wipe off any excess water from the bone sample.
 - b. Calculate density $\rho = \text{mass/volume}$. Density values should range from 1.5 – 3.0 g/cm³. (1,500- 3,000 kg/m³)

PART TWO: INTIAL SETUP AND CALIBRATION

4. Attach the power cord to the side of the device and plug in.
5. Connect the transducer wire to either of the two ports on the top of the device to the low frequency transducer that best fits the sample. For this lab, we will be using the V110 transducer. Writing on the transducer should face up when touching the surface of the sample.
6. Press the green ON/OFF button on the Panametrics NDT device.
7. Calibrate the machine using the steel sample. While this will not be used for your lab, the purpose is to familiarize you with the proper functioning of the equipment.

- a. Once you turn on the machine, wait until you see the graphical display appear before you press any of the other buttons.
Press the yellow ZERO OFFSET button. Then press F1. Add enough mineral oil (coupling agent) to the calibration plate to cover the entire surface of the calibration sample. There are Q-Tips to use for applying the oil.
- b. Place the transducer on the steel calibration disk. The transducer should be held tightly against the sample throughout the calibration. If machine is displaying a large amount of noise or not functioning properly consult instructor.
- c. Be sure setting is on peak to peak for steel sample calibration. To check this, look at far right side in about the middle of the display there is white icon that displays 2 peaks. If it only shows one peak, press the white 2nd button in the bottom left corner and then press the orange DEPTH/%AMP key with white writing “echo-echo” above it.

RANGE

8. Push the yellow RANGE button.
9. Select the appropriate range from the white F1-F5 keys (located at the top of the pad). Choose the range where you can clearly see two distinct peaks excluding the 1st cluster of peaks on the far left of the display. (Figure 1)



Figure 1: F1-F5 buttons

GAIN

10. Press the blue GAIN button.
11. Select the appropriate gain from the white F1-F5 keys. The two distinct peaks should still be visible on the screen.

LOCATION OF GATES

12. Press the red GATE 1 button.
13. Use the green up, down, right and left to place the solid red gate centered and near but not at the top of the first visible peak.
14. Press the red GATE 2 button. Use the green up, down, right and left to place the outlined red gate centered and near but on at the top of the second visible peak.
15. Press the yellow CALIBRATION button.

VELOCITY

16. Press the yellow VEL button. A window should appear.
17. Enter the actual thickness of the sample by using the yellow key pad. Press the purple ENTER button.
18. Record the velocity value from the display.

PART THREE: TEST BONE SAMPLES

19. Measure thickness of bone samples in all directions using calipers.
20. Place lateral bone sample (labeled “L”) on the steel calibration platform with the “x” facing up (1,1 direction).
21. Put coupling agent on the “x” face bone sample.
22. Press the yellow ZERO OFFSET button.
23. Press F1.
24. Change setting to “echo-echo” by pressing 2nd function then the orange DEPTH/% AMP key. The white icon on the display should indicate 1 peak.
25. Place transducer upon that same surface. The transducer should be held tightly against the bone throughout the test.
26. The following steps should be repeated for the bone in the same manner as was conducted during the calibration of the steel samples.
 - a. Adjust the range:
 - b. Adjust the gain:
 - c. Adjust location of the gate:
 - d. Adjust the velocity:
 - i. Press the yellow VEL button. (velocity) A window should appear.
 - ii. Enter the actual thickness of the sample in the 1,1 direction by using the yellow key pad and press the purple ENTER button.
27. Record the velocity of sound through the material from the display.
28. Using density and the velocity, calculate the stiffness coefficient of the bone sample:
Stiffness Coefficient: $C_{ii} = \rho * V_{ii}^2$
where ρ is the apparent density (kg/m^3) of the material and V_{ii} is the longitudinal velocity (m/s). Record the calculated values on the data table.
29. Repeat steps 6-7 for the remaining 2,2 (“y”) and 3,3 (“.”) lateral directions.
30. Repeat steps 6-8 for the remaining medial, cranial and/or caudal samples in all three directions.
31. Turn off all equipment and cleanup workstation.
32. Calculate the average and standard deviations.
33. Compare obtained stiffness coefficient experimental value with accepted literature values as below.

Longitudinal Velocity ranged from:

2700-4200 m/s

Stiffness Coefficient ranged from:

14-21 GPA in the Lateral and Medial directions

20-25 GPA in the Cranial and Caudal directions

34. Statistically compare the values of the stiffness coefficients $C_{i,i}$ in the three principle directions in the lateral, medial, cranial and caudal samples using a one-way ANOVA in Minitab. This means you will run three one-way ANOVA tests. Below is the procedure for performing a One-Way ANOVA using Minitab courtesy of Dr. Jim Doi.
35. Say acceptable risk is 5%, therefore if the p-value is less than 0.05, there is at least one significant difference among the stiffness coefficients at different relative positions of bone.

One-Way or Single-Factor ANOVA:

Suppose you have data according to the following four treatments (L1 -- L4):

L1 85.06 85.25 84.87

L2 84.99 84.28 84.88

L3 84.48 84.72 85.10

L4 84.10 84.55 84.05

For this lab the L1 values for the $C_{1,1}$ test will consist of the three $C_{1,1}$ values of the lateral sample. The L2 values for the $C_{1,1}$ test will consist of the three $C_{1,1}$ values of the medial sample. The L3 values for the $C_{1,1}$ test will consist of the three $C_{1,1}$ values of the cranial sample. The L4 values for the $C_{1,1}$ test will consist of the three $C_{1,1}$ values of the caudal sample. Follow this same procedure for the $C_{2,2}$ and $C_{3,3}$.

36. Input this data in one of the following ways:

For Method 1, we input the levels of the treatment in one column (C1) and the corresponding values of the response variable in another column (C2). This is called the stacked method in Minitab.

For Method 2, we input the response values of a given treatment in a unique column. The data for treatments L1 through L4 are stored in columns C4 through C7 respectively. See image:

	C1-T	C2	C3	C4	C5	C6	C7
				L1	L2	L3	L4
1	L1	85.06		85.06	81.99	87.78	87.13
2	L1	85.26		85.26	81.28	87.72	87.55
3	L1	81.87		81.87	81.88	86.10	87.35
4	L2	81.55					
5	L2	81.26					
6	L2	81.11					
7	L2	81.11					
8	L2	81.72					
9	L2	86.11					
10	L2	81.11					
11	L2	81.11					
12	L2	81.11					

Figure 1: MiniTab data analysis example.

37. To perform the One-way ANOVA in Minitab for Method 1, click on Stat -> ANOVA -> One Way.
38. In the dialogue box which appears, select the appropriate column for 'Response' (C2). For 'Factor', select the appropriate column which contains the treatment levels (C1). Click on OK to generate the result of the hypothesis test.
39. To perform the One-way ANOVA in Minitab for Method 2, click on Stat -> ANOVA -> One Way
40. (Unstacked). In the dialogue box which appears, select the appropriate column for 'Response' (C2). For 'Factor', select the appropriate column which contains the treatment labels (C1). Click on OK to generate the result of the hypothesis test.
41. Both methods will, of course, yield the same output. See below for the corresponding result for the given data set:

```

One-way ANOVA: C2 versus C1
Source  DF      SS      MS      F      P
C1          3    1.0559  0.3520  3.96    0.053
Error       8    0.7114  0.0889
Total     11    1.7673
S = 0.2982    R-Sq = 59.75%    R-Sq(adj) = 44.65%
Individual 95% CIs For Mean Based on

```

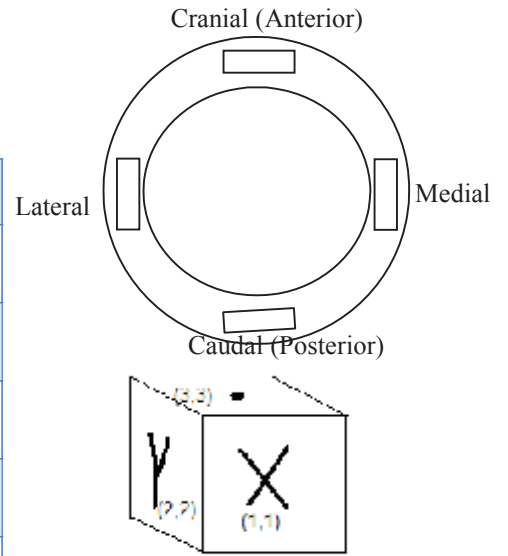
Pooled StDev			
Level	N	Mean	StDev
L1	3	85.060	0.190
(-----*-----)			
		L2	3 84.717 0.382
(-----*-----)			
L3	3	84.767	0.313
(-----*-----)			
		L4	3 84.233
(-----*-----)			
0.275			
84.00	84.50	85.00	85.50
Pooled StDev = 0.29			

1. What are the advantages of using ultrasonic techniques for measuring the elastic properties of bone?
2. What is anisotropy?
3. Why are the elastic properties of bone so directionally dependent?
4. Why do you want to use a low frequency wavelength to measure the elastic properties of bone when higher frequencies are typically used for other material analysis?
5. How do your results compare with the accepted literature values? If they vary, why do you think this is? Give some possible reasons why your results might not be consistent with the literature values.

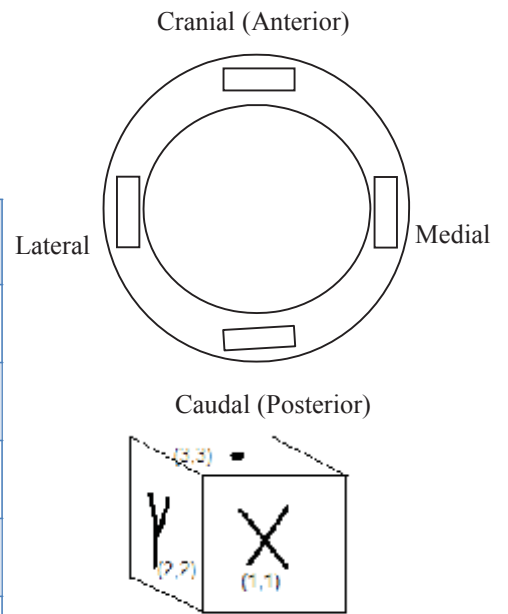
1. T. Nelligan, "An Introduction to Ultrasonic Material Analysis." .
2. J.Y. Rho, "An Ultrasonic Method for Measuring the Elastic Properties of Human Tibial Cortical and Cancellous Bone." *Ultrasonics* 34: 777-783, 1996.
3. NDT Resource Center. "Piezoelectric Transducers"
4. NDT Resource Center. "Basic Principles of Ultrasonic Testing"
5. J.Y Rho, M.C. Hobatho, R.B. Ashman, "Relations of Mechanical Properties to Density and CT Numbers in Human Bone" *Med. Eng. Phys.* 17 No.5: 347-355, 1995.
6. G. Haiat, "Numerical Simulation of the Dependence of Quantitative Ultrasonic Parameters on Trabecular Bone Microarchitecture and Elastic Constants." *Ultrasonics* 44: 289-294, 2006.
7. S.P. Kotha, "High Frequency Ultrasound Prediction of Mechanical Properties of Cortical Bone with Varying Amount of Mineral Content". *Ultrasound in Med & Biol.* 33, 2007.
8. K. Raum, "Bone Microstructure and Elastic Tissue Properties are Reflected in Qus Axial Transmission Measurements." *Ultrasound in Med & Biol.* 31 Number 9: 1225-1235, 2005.
9. S. Bensamoun, "Spatcial Distribution of Acoustic and Elastic Properties of Human Femoral Cortical Bone." *Journal of Biomechanics* 37: 503-510, 2004.
10. "Advanced Detection of Bone Quality." *Journal of Biomechanics* 39: 465.
11. H. Guelcher, [An Introduction to Biomaterials](#). CRC Press. 369-393, 2006.
12. P. Lasaygues, M. Pithioux, "Ultrasonic Characterization of Orthotropic Elastic Bovine Bones." *Ultrasonics* 39: 567-573, 2002.

APPENDIX – SAMPLE DATA TABLE

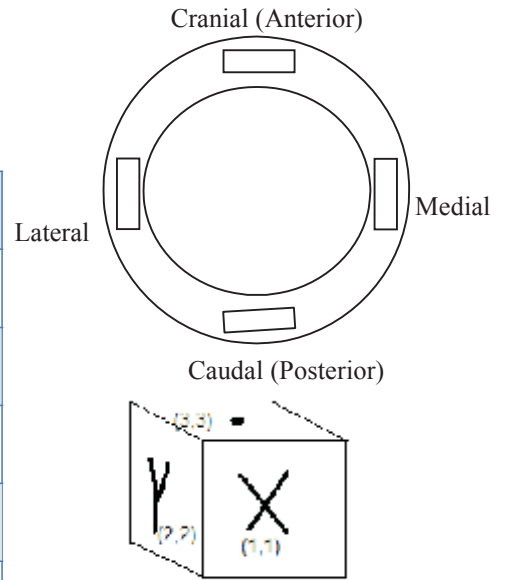
Lateral Sample	1	2	3		
Weight(kg)					
Displacement (mL)					
Density (kg/m ³)					
Thickness _{1,1} (mm)					
Thickness _{2,2} (mm)					
Thickness _{3,3} (mm)				Average	Std. Dev.
V _{1,1} (m/s)					
V _{2,2} (m/s)					
V _{3,3} (m/s)					
C _{1,1} (GPa)*					
C _{2,2} (GPa)*					
C _{3,3} (GPa)*					



Cranial Sample	1	2	3		
Weight(kg)					
Displacement (mL)					
Density (kg/m ³)					
Thickness _{1,1} (mm)					
Thickness _{2,2} (mm)					
Thickness _{3,3} (mm)				Average	Std. Dev.
V _{1,1} (m/s)					
V _{2,2} (m/s)					
V _{3,3} (m/s)					
C _{1,1} (GPa)*					
C _{2,2} (GPa)*					
C _{3,3} (GPa)*					



Caudal Sample	1	2	3		
Weight(kg)					
Displacement (mL)					
Density (kg/m ³)					
Thickness _{1,1} (mm)					
Thickness _{2,2} (mm)					
Thickness _{3,3} (mm)				Average	Std. Dev.
V _{1,1} (m/s)					
V _{2,2} (m/s)					
V _{3,3} (m/s)					
C _{1,1} (GPa)*					
C _{2,2} (GPa)*					
C _{3,3} (GPa)*					



Medial Sample	1	2	3		
Weight(kg)					
Displacement (mL)					
Density (kg/m ³)					
Thickness _{1,1} (mm)					
Thickness _{2,2} (mm)					
Thickness _{3,3} (mm)				Average	Std. Dev.
V _{1,1} (m/s)					
V _{2,2} (m/s)					
V _{3,3} (m/s)					
C _{1,1} (GPa)*					
C _{2,2} (GPa)*					
C _{3,3} (GPa)*					

